INTERNATIONAL ATOMIC ENERGY AGENCY
UNITED NATIONS EDUCATIONAL, SCIENTIFIC AND CULTURAL ORGANIZATION
INTERNATIONAL CENTRE FOR THEORETICAL PHYSICS
I.C.T.P., P.O. BOX 586, 34100 TRIESTE, ITALY, CABLE: CENTRATOM TRIESTE

H4.SMR/480-8

WORKSHOP ON EARTHQUAKE SOURCES & REGIONAL LITHOSPHERIC STRUCTURES FROM SEISMIC WAVE DATA

19 - 30 November 1990

Synthetic Seismograms from Multimode Summation - Theory & Computational Aspects

G. F. Panza

Istituto di Geodesia e Geofisica
Università di Trieste,

International Center for Earth & Environmental Sciences

SYNTHETIC SEISMOGRAMS FROM MULTIMODE SUMMATION.- THEORY AND COMPUTATIONAL ASPECTS

G.F. PANZA
Istituto di Geodesia e Geofisica - Università di Trieste - ITALY
International Center for Earth and Environmental Sciences - Miramar - ITALY

Summary

From the latest developments of algorithms for the computation of eigenvalues and eigenfunctions of Love (SH) and Rayleigh (P-SV) waves for flat anelastic layered media, it is possible to construct, with highly satisfactory efficiency and accuracy, complete broad-band synthetic seismograms. Therefore, computer programs based on the addition of modes are quite versatile and can be used to model, in a realistic way, seismological and seismic signals, also for laterally heterogeneous media.

1. INTRODUCTION

In spite of the very considerable efforts made by seismologists and theoreticians, it is still missing a satisfactory theory which describes accurately wave propagation in three-dimensional models of the Earth. If the extremely time consuming numerical procedures, based on finite differences or finite element methods, are excluded, all the existing analytical methods involve significant approximations. The modal summation method (1,2) is practically free from approximation in the one dimensional case and can be efficiently extended, introducing approximations of variable and to some extent quantifiable size, to two- and three-dimensional cases (3). The method allows to construct very realistic signals, also in the relatively simple one-dimensional case, and can be very easily applied for a quantitative and realistic earthquake hazard assessement.

2. WAVES IN MULTILAYERED MEDIA

The medium is assumed to consist of homogeneous layers, separated by first-order discontinuities. If a medium is continuously inhomogeneous, it

is replaced by a number of homogeneous layers; in smooth gradient zones it is usually sufficient to choose roughly half the dominant wavelength as layer thickness, whereas in transition zones with larger velocity gradients the layer thickness should be reduced further. The advantage of the homogeneous-layer approximation is that inside each layer the equation of motion takes a relatively simple form and can be solved exacly. Its disadvantage is that boundary conditions have to be fulfilled at many interfaces. Analytical methods for inhomogeneous layers - in contrast to numerical, e.g. finite-difference methods - are not yet developed to a point where they really can compete with the methods for homogeneous layers. At present, within the frame of ICTP-ICE-IGG activities, it is under development a large project for the formulation of the theory and related computer code for the construction of complete synthetic seismograms for three-dimensional anelastic media, based on modal summation.

The equation of motion for a homogeneous, isotropic elastic medium is

$$\rho u_{tt} = (\lambda+2\mu)\ \text{grad div}\ u - \text{rot rot}\ u \qquad (1)$$

where u is the displacement vector, u_{tt} its time second order derivative, ρ is the density and λ and μ are the Lamé parameters. Body forces due to gravity and seismic sources are not included in equation (1): it is assumed that gravity has no other effect than to determine, via self compression, the constant values of ρ, λ and μ, and sources of seismic waves are included through their known contribution to u (4). In order to simplify the discussion as far as possible, we shall consider solutions of the elastic equations of motion in the form of plane waves rather than attempt to treat the more complex case of waves diverging from a point-source. This does not involve loss of generality in the computation of the dispersion function since the point-source solution may be developed by integration of plane-wave solutions (4), with a preassigned precision depending upon source-receiver distance (5).

Let us consider plane waves of angular frequency ω and horizontal phase velocity c propagated in a semi-infinite medium made up of n parallel, homogeneous, isotropic layers. The x axis is taken parallel to the layers with the positive sense in the direction of propagation. The positive z axis is taken as directed into the medium. The various layers and interfaces are numbered away from the free surface, as shown in Figure 1. We treat first waves of Rayleigh type (P-SV motion), by which we mean that there is no displacement in the y direction and that the amplitude diminishes exponentially in the positive z direction in the semi-infinite layer. The case of waves of Love type (SH motion) is treated in section 4.

3. P-SV WAVES

For the m-th layer let ρ_m= density, d_m= thickness, λ_m and $\mu_m = \rho_m \beta_m^2$= Lamé elastic constants, α_m= velocity of propagation of dilatational waves, β_m=velocity of propagation of rotational waves, $k=\omega/c$=horizontal wave number, $\gamma_m = 2(\beta_m/c)^2$, u_m=displacement component in the x direction, w_m=displacement component in the z direction, σ_m=normal stress, τ_m=tangential stress.

For $m<n$ $r_{\alpha_m}=[(c/\alpha_m)^2-1]^{1/2}$ if $c>\alpha_m$ and $r_{\alpha_m}=-i[1-(c/\alpha_m)^2]^{1/2}$, if $c<\alpha_m$; furthermore $r_{\beta_m}=[(c/\beta_m)^2-1]^{1/2}$, if $c>\beta_m$ and $r_{\beta_m}=-i[1-(c/\beta_m)^2]^{1/2}$ if $c<\beta_m$. Finally, if $m=n$, $r_{\alpha_m}=-i[1-(c/am)^2]^{1/2}$ and $r_{\beta_m}=-i[1-(c/\beta_m)^2]^{1/2}$.

Then periodic solutions of the elastic equation of motion for the m-th layer may be found by combining dilatational wave solutions,

$$\Delta_m=(\partial u_m/\partial x)+(\partial w_m/\partial z)= \exp[i(pt-kx)][\Delta'_m \exp(-ikr_{\alpha_m}z)+\Delta''_m \exp(ikr_{\alpha_m}z)] \qquad (2)$$

with rotational wave solutions

$$\delta_m=(1/2)[(\partial u_m/\partial z)-(\partial w_m/\partial x)]= \exp[i(pt-kx)][\delta'_m \exp(-ikr_{\beta_m}z)+\delta''_m \exp(ikr_{\beta_m}z) \qquad (3)$$

where Δ'_m, Δ''_m, δ'_m and δ''_m are constants.

With the sign conventions defined above, the term in Δ'_m represents a plane wave whose direction of propagation makes an angle $\cot^{-1} r_{\alpha_m}$ with the +z direction when r_{α_m} is real, and a wave propagated in the +x direction with amplitude diminishing exponentially in the +z direction when r_{α_m} is imaginary. Similarly, the term in Δ''_m represents a plane wave making the same angle with the -z direction when r_{α_m} is real and a wave propagated in the +x direction with amplitude increasing exponentially in the +z direction when r_{α_m} is imaginary. The same applies to the terms in δ'_m and δ''_m with r_{β_m} substituted for r_{α_m} (see Figures 2a, 2b, 2c, 2d).

Droping the term $\exp[i(\omega t-kx)]$ the displacements and the pertinent stress components corresponding to the dilatation and rotation, given by equations (2) and (3), can be written:

$$m=-(\alpha_m/\omega)^2(\partial\Delta_m/\partial x)-2(\beta_m/\omega)^2(\partial\delta_m/\partial z) \quad (4)$$

$$m=-(\alpha_m/\omega)^2(\partial\Delta_m/\partial z)+2(\beta_m/\omega)^2(\partial\delta_m/\partial x) \quad (5)$$

$$m=\rho_m\{\alpha^2{}_m\Delta_m+2\beta^2{}_m[(\alpha_m/\omega)^2(\partial^2\Delta_m/\partial x^2)+2(\beta_m/\omega)^2(\partial^2\delta_m/\partial x\partial z)]\} \quad (6)$$

$$n=2\rho_m\beta^2{}_m\{-(\alpha_m/\omega)^2(\partial^2\Delta_m/\partial x\partial z)+(\beta_m/\omega)^2[(\partial^2\delta_m/\partial x^2)-(\partial^2\delta_m/\partial z^2)]\} \quad (7)$$

he boundary conditions at an interface between two layers require that ese four quantities should be continuous. Continuity of the displacements is sured if the corresponding velocity components $\dot{u}_m$ and $\dot{w}_m$ are made ntinuous and, since c is the same in all layers, we may take the mensionless quantities $\dot{u}_m/c$ and $\dot{w}_m/c$ to be continuous. Substituting the pressions (2) and (3) in equations (4) to (7) and expressing the exponential nctions of ikrz in trigonometric form, we find

$$\dot{u}_m=A_m\cos p_m-iB_m\sin p_m+r_{\beta_m}C_m\cos q_m-ir_{\beta_m}D_m\sin q_m \quad (8)$$

$$\dot{w}_m=-ir_{\alpha_m}A_m\sin p_m+r_{\alpha_m}B_m\cos p_m+iC_m\sin q_m-D_m\cos q_m \quad (9)$$

$$n=\rho_m(\gamma_m-1)A_m\cos p_m-i\rho_m(\gamma_m-1)B_m\sin p_m+\rho_m\gamma_m r_{\beta_m}C_m\cos q_m-i\rho_m\gamma_m r_{\beta_m}D_m\sin q_m \quad (10)$$

$$=i\rho_m\gamma_m r_{\alpha_m}A_m\sin p_m-\rho_m\gamma_m r_{\alpha_m}B_m\cos p_m-i\rho_m(\gamma_m-1)C_m\sin q_m+\rho_m(\gamma_m-1)D_m\cos q_m \quad (11)$$

here

$m=-\alpha^2{}_m(\Delta'_m+\Delta''_m)$, $B_m=-\alpha^2{}_m(\Delta'_m-\Delta''_m)$, $C_m=-2\beta^2{}_m(\delta'_m-\delta''_m)$, $D_m=-2\beta^2{}_m(\delta'_m+\delta''_m)$, $n=kr_{\alpha_m}[z-z^{(m-1)}]$, $q_m=kr_{\beta_m}[z-z^{(m-1)}]$, $z^{(m-1)}$ is the depth of the upper interface the m-th layer and Δ'_m, Δ''_m, δ'_m, δ''_m are the constants defined in (6) pearing in the depth-dependent part of the dilatational and rotational wave lutions:

$$'_m\exp(-ikr_{\alpha_m}z)+\Delta''_m\exp(ikr_{\alpha_m}z) \quad (12)$$

$$_m\exp(-ikr_{\beta_m}z)+\delta''_m\exp(ikr_{\beta_m}z) \quad (13)$$

1. EVALUATION OF EIGENVALUES AND EIGENFUNCTIONS

For a continental model, the vanishing of the two components of stress the free surface yields:

$$t(\gamma_1-1)A_1-\rho_1\gamma_1 r_{\beta_1}C_1=0 \quad (14)$$

$$\gamma_1 r_{\alpha_1}B_1-\rho_1(\gamma_1-1)A_1=0 \quad (15)$$

Thus the submatrix $A^{(0)}$ defined in (7,8) can be written in the form

$$A^{(0)}=\begin{vmatrix} -\rho_1(\gamma_1-1) & 0 & -\rho_1\gamma_1 & 0 \\ 0 & \rho_1\gamma_1 & 0 & -\rho_1(\gamma_1-1) \end{vmatrix} \quad (16)$$

At the m-th interface, the continuity of displacement and stress yields

$$A_m\cos P_m-iB_m\sin P_m+r_{\beta_m}C_m\cos Q_m-ir_{\beta_m}D_m\sin Q_m=A_{m+1}+r_{\beta_{m+1}}C_{m+1}, \quad (17)$$

$$-ir_{\alpha_m}A_m\sin P_m+r_{\alpha_m}B_m\cos P_m+iC_m\sin Q_m-D_m\cos Q_m=r_{\alpha_{m+1}}Bm+1-Dm+1 \quad (18)$$

$$\rho_m(\gamma_m-1)A_m\cos P_m-i\rho_m(\gamma_m-1)B_m\sin P_m+\rho_m\gamma_m r_{\beta_m}C_m\cos Q_m-i\rho_m\gamma_m r_{\beta_m}D_m\sin Q_m=\rho_{m+1}(\gamma_{m+1}-1)A_{m+1}+\rho_{m+1}\gamma_{m+1}r_{\beta_{m+1}}C_{m+1}, \quad (19)$$

$$i\rho_m\gamma_m r_{\alpha_m}A_m\sin P_m-\rho_m\gamma_m r_{\alpha_m}B_m\cos P_m-i\rho_m(\gamma_m-1)C_m\sin Q_m+\rho_m(\gamma_m-1)D_m\cos Q_m=\rho_{m+1}\gamma_{m+1}r_{\alpha_{m+1}}B_{m+1}+\rho_{m+1}(\gamma_{m+1}-1)D_{m+1} \quad (20)$$

where $P_m=kr_{\alpha_m}d_m$, $Q_m=kr_{\beta_m}d_m$ and d_m is the layer thickness. Thus the interface submatrices defined in (6) have the form

$$A^{(m)}=\begin{vmatrix} \cos P_m & -i\sin P_m/r_{\alpha_m} & \cos Q_m & -ir_{\beta_m}\sin Q_m \\ -ir_{\alpha_m}\sin P_m & \cos P_m & i\sin Q_m/r_{\beta_m} & -\cos Q_m \\ \rho_m(\gamma_m-1)\cos P_m & -i\rho_m(\gamma_m-1)\sin P_m/r_{\alpha_m} & \rho_m\gamma_m\cos Q_m & -i\rho_m\gamma_m r_{\beta_m}\sin Q_m \\ i\rho_m\gamma_m r_{\alpha_m}\sin P_m & -\rho_m\gamma_m\cos P_m & -i\rho_m(\gamma_m-1)\sin Q_m/r_{\beta_m} & \rho_m(\gamma_m-1)\cos Q_m \end{vmatrix}$$

$$\begin{vmatrix} -1 & 0 & -1 & 0 \\ 0 & -1 & 0 & 1 \\ -\rho_{m+1}(\gamma_{m+1}-1) & 0 & -\rho_{m+1}\gamma_{m+1} & 0 \\ 0 & \rho_{m+1}\gamma_{m+1} & 0 & -\rho_{m+1}(\gamma_{m+1}-1) \end{vmatrix} \quad (21)$$

and, noting that, when imposing surface waves conditions, in the half space $\Delta''_n=\delta''_n=0$, $A_n=B_n=-\alpha^2{}_n\Delta'_n$ and $C_n=D_n=-2\beta_n\omega'_n$, the submatrix representing the (n-1)th interface has the form

$$A^{(n-1)}=\begin{vmatrix} \ldots & -1 & -r_{\beta_n} \\ \ldots & -r_{\alpha_n} & 1 \\ \ldots & -\rho_n(\gamma_n-1) & -\rho_n\gamma_n r_{\beta_n} \\ \ldots & \rho_n\gamma_n r_{\alpha_n} & -\rho_n(\gamma_n-1) \end{vmatrix} \quad (22)$$

where the first four columns are the same as those of $\Lambda^{(m)}$ with m=n-1. For each layer, $\Lambda^{(i)}$ (i=1,n) submatrices represent the denominators of Cramer's system solutions when the boundary conditions are applied. In more compact notation it can be written

$$\Delta_R = \begin{vmatrix} |\Lambda^{(0)}| & & & & \\ & |\Lambda^{(1)}| & & & \\ & & |\cdot| & & \\ & & & |\Lambda^{(n-2)}| & \\ & & & & |\Lambda^{(n-1)}| \end{vmatrix} \qquad (23)$$

where the non zero elements only are pictured. A condition for surface waves to exist is $\Delta_R=0$, which defines the dispersion function for Rayleigh waves:

$$F_R(\omega,c)=\Delta_R=0. \qquad (24)$$

The discrete solutions (ω,c) of the equation (24) describe, in each of the layers, body waves or surface waves depending upon the real or imaginary nature of r_{α_m} and r_{β_m}. More precisely real values of r_{α_m} and r_{β_m} correspond to P- and S-waves while imaginary values of r_{α_m} and r_{β_m} correspond to surface waves. Therefore the modal summation method allows to solve in an exact and complete way the full wave equation in a preassigned (ω,c) interval. In other words it is possible to describe all the rays propagating with phase velocity less than a preassigned maximum value. It is easy to prove that using the modal representation the upper limit for the phase velocity is represented by the S-wave velocity value assigned to the half space used to terminate the structure at depth.

Once the eigenvalue problem is solved it is possible to determine eigenfunctions, i.e. displacements and stresses.

The algorithmic details of eigenfunction evaluation by Knopoff's method are rather involved (9) and here details will be given only for SH-waves (see section 4.1). The problem consist in the determination of the constants A_m,B_m,C_m,D_m for the layers above the homogeneous half-space and the constants A_n and D_n for the deepest structural unit. The starting point is therefore the linear, homogeneous system of 4n-2 equations in 4n-2 unknowns

$$\begin{vmatrix} |\Lambda^{(0)}| & & & \\ & |\Lambda^{(1)}| & & \\ & & |\cdot| & \\ & & & |\Lambda^{(n-1)}| \end{vmatrix} \begin{vmatrix} A_1 \\ r_{\alpha_1}B_1 \\ r_{\beta_1}C_1 \\ D_1 \\ A_2 \\ r_{\alpha_2}B_2 \\ r_{\beta_2}C_2 \\ D_2 \\ \\ A_{n-1} \\ r_{\alpha_{n-1}}B_{n-1} \\ r_{\beta_{n-1}}C_{n-1} \\ D_{n-1} \\ A_n \\ D_n \end{vmatrix} = \begin{vmatrix} 0 \\ 0 \\ 0 \\ 0 \\ \\ \\ \\ \\ \\ \\ \\ \\ 0 \\ 0 \end{vmatrix} \qquad (25)$$

where the submatrices $\Lambda^{(i)}$ (i=1,n) are given by equations (16), (21) and (22). Once the dispersion or eigenvalue problem is solved we are ready to determine the layer constants. This is done by deleting the last equation of the system and transposing the terms containing D_n to the right-hand side of the equations, thus forming a vector of inhomogeneous terms. If we arbitralily set D_n to unity, this will force all $r_{\alpha_m}B_m$ and D_m to be real, and all A_m and $r_{\beta_m}C_m$ to be imaginary. At this stage Cramer's rule can be applied to obtain A_n. The remaining layer constants can be determined by iteration. For more details about the computations of eigenfunctions see (9).

4. SH WAVES

With the same notations and geometry of section 3 we may write, for the m-th layer, the following expressions for the displacement and the stress

$$u_m=w_m=\sigma_m=\tau_m=0 \qquad (26)$$

$$v_m=\exp i(\omega t-kx)[v'_m\exp(-ik\beta_m z)+v''_m\exp(ik\beta_m z)] \qquad (27)$$

$$\upsilon_m=\mu_m(\partial v_m/\partial z)=ik\mu_m r_{\beta_m}\exp i(\omega t-kx)[v''_m\exp(ik\beta_m z)-v'_m\exp(-ik\beta_m z)] \qquad (28)$$

Neglecting, here too, the term exp i(ωt-kx), at the m-th interface the continuity of displacement and stress yields

$$\dot{v}_m/c=(\dot{v}_{m-1}/c)\cos Q_m+iu_{m-1}(m_m r_{\beta_m})^{-1}\sin Q_m \qquad (29)$$

$$u_m=i(\dot{v}_{m-1}/c)m_m r_{\beta_m}\sin Q_m+u_{m-1}\cos Q_m \qquad (30)$$

4.1. EVALUATION OF EIGENVALUES AND EIGENFUNCTIONS

From eqations (29) and (30) the layer matrix can be defined:

$$a_m=\begin{bmatrix} \cos Q_m & \dfrac{i\sin Q_m}{\mu_m \cdot r_{\beta_-}} \\ i\mu_m \cdot r_{\beta_-} \cdot \sin Q_m & \cos Q_m \end{bmatrix} \qquad (31)$$

For the multimode surface-wave eigenvalue computations, using notation of (8), the dispersion function can be written as the modified product for layer-matrices :

$$F_L(\omega, c)=b_n \cdot b_{n-1} \cdot b_{n-2} \cdot \ldots\ldots b_1 \qquad (31)$$

where n is the number of layers, including the lower halfspace. In equation (31) b_n is given by:

$b_n=(s,-1)$ if the halfspace is solid
$b_n=(0,-1)$ if the halfspace is liquid (32)
$b_n=(1,0)$ if the halfspace is rigid

where

$$s=-\mu_n \cdot \left(1-\left(\frac{c}{\beta_n}\right)^2\right)^{\frac{1}{2}} \qquad (33)$$

b_m (0<m<n) is given by:

$$b_m=\begin{bmatrix} \cos Q_m & \dfrac{\sin Q_m}{\mu_m \cdot r_{\beta_m}} \\ \mu_m \cdot r_{\beta_m} \cdot \sin Q_m & \cos Q_m \end{bmatrix} \qquad \text{if } c > \beta_m \qquad (34)$$

$$b_m=\begin{bmatrix} \cosh Q^*_m & \dfrac{\sinh Q^*_m}{\mu_m \cdot r^*_{\beta_-}} \\ -\mu_m \cdot r^*_{\beta_-} \cdot \sinh Q^*_m & \cosh Q^*_m \end{bmatrix} \qquad \text{if } c < \beta_m \qquad (35)$$

$$b_m=\begin{bmatrix} 1 & \dfrac{p \cdot d_m}{\mu_m \cdot c} \\ 0 & 1 \end{bmatrix} \qquad \text{if } c=\beta_m \qquad (36)$$

where we have introduced the real part of imaginary quantities

$$\left.\begin{aligned} r^*_{\beta_-} &= -\left(1-\left(\frac{c}{\beta_m}\right)^2\right)^{\frac{1}{2}} \\ Q^*_m &= \frac{p \cdot r^*_{\beta_-} \cdot d_m}{c} = k \cdot r^*_{\beta_-} \cdot d_m \end{aligned}\right\} \quad \text{if } c < \beta_m \qquad (37)$$

The modified matrix product of b_m and b_{m-1} is defined as follows:

$$[b_m \cdot b_{m-1}]_{jk}=\begin{cases} (b_m)_{jl} \cdot (b_{m-1})_{lk} & \text{if } (j+k) \text{ is even} \\ (-1)^{j+1} \cdot (b_m)_{jl} \cdot (b_{m-1})_{lk} & \text{if } (j+k) \text{ is odd} \end{cases} \qquad (38)$$

The mathematical solution of the surface wave propagation allows two types of waves in the solid halfspace, exponentially increasing and decreasing with depth. To avoid infinite values of the solution, the coefficient of exponentially increasing wave in the halfspace must vanish (surface waves condition). If the halfspace is supposed to be liquid, the deepest interface is at the analogy of the mantle-core boundary. In analogy with the case of P-SV waves, imaginary values of r_{β_m} correspond to surface waves, while real values of r_{β_m} correspond to S-waves. More precisely real values of r_{β_m} correspond to S-waves while imaginary values of r_{β_m} correspond to surface waves. Therefore also for SH-waves, the modal summation method allows to solve in an exact and complete way the full wave equation in a preassigned (ω,c) interval. In other words it is possible to describe all the rays propagating with phase velocity less than a preassigned maximum value. It is easy to prove that using the modal representation the upper limit for the phase velocity is represented by the S-wave velocity value assigned to the half space used to terminate the structure at depth.

With the geometry shown in Figure 1, the computation of the eigenfunctions at the layer interfaces can be performed as follows (10):

$$\begin{bmatrix} v_m \\ \upsilon_m \end{bmatrix} = \begin{bmatrix} \cos Q_m & \dfrac{\sin Q_m}{k \cdot \mu_m \cdot r_{\beta_m}} \\ -k \cdot \mu_m \cdot r_{\beta_m} \cdot \sin Q_m & \cos Q_m \end{bmatrix} \cdot \begin{bmatrix} v_{m-1} \\ \upsilon_{m-1} \end{bmatrix} \quad \text{if } c > \beta_m \qquad (39)$$

$$\begin{bmatrix} v_m \\ \upsilon_m \end{bmatrix} = \begin{bmatrix} \cosh Q^*_m & \dfrac{\sinh Q^*_m}{k \cdot \mu_m \cdot r^*_{\beta_m}} \\ k \cdot \mu_m \cdot r^*_{\beta_m} \cdot \sinh Q^*_m & \cosh Q^*_m \end{bmatrix} \cdot \begin{bmatrix} v_{m-1} \\ \upsilon_{m-1} \end{bmatrix} \quad \text{if } c < \beta_m \qquad (40)$$

$$\begin{bmatrix} v_m \\ \upsilon_m \end{bmatrix} = \begin{bmatrix} 1 & \dfrac{d_m}{\mu_m} \\ 0 & 1 \end{bmatrix} \cdot \begin{bmatrix} v_{m-1} \\ \upsilon_{m-1} \end{bmatrix} \quad \text{if } c = \beta_m \qquad (41)$$

where v_m is the displacement and υ_m the stress at the interface m. Notice that :

$$\dot{v}_m = i\omega v_m \qquad (42)$$

For the last interface, supposing a solid terminating halfspace, we shall use:

$$v_{n-1} = \begin{cases} v_{n-2} \cdot \cos Q_{n-1} + \dfrac{\upsilon_{n-2} \cdot \sin Q_{n-1}}{k_{n-1} \cdot r_{\beta_{n-1}} \cdot \mu_{n-1}} & \text{if } c > \beta_{n-1} \\ v_{n-2} \cdot \cos Q^*_{n-1} + \dfrac{\upsilon_{n-2} \cdot \sin Q^*_{n-1}}{k_{n-1} \cdot r^*_{\beta_{n-1}} \cdot \mu_{n-1}} & \text{if } c < \beta_{n-1} \\ v_{n-2} + \upsilon_{n-2} \cdot \dfrac{d_{n-1}}{\mu_{n-1}} & \text{if } c = \beta_{n-1} \end{cases} \qquad (43)$$

These computations are performed using the initial values $(v_0, \upsilon_0) = (1,0)$ at the free surface.

5. COMPUTATION OF GROUP VELOCITIES

Following (8) the group velocity, u, is obtained from

$$u = \frac{c}{1-(\omega/c)(\partial c/\partial \omega)} \qquad (44)$$

where standard implicit function theory is applied to the dispersion function F to obtain

$$dc/d\omega = -(\partial F/\partial \omega)_c / (\partial F/\partial c)_\omega \qquad (45)$$

Equation (45) is obviously valid both when F indicates Love as well as Rayleigh dispersion function. Details about the analytic computation of (45) are given for Love waves in appendix A.

6. ENERGY INTEGRAL

Along with eigenvalues and eigenfunctions, the integrals:

$$I_{I_R} = \int_0^{\infty} \rho(z)[y^2_1(z) + y^2_3(z)]dz \qquad (46)$$

or Rayleigh waves, and

$$I_{I_L} = \int_0^{\infty} \rho(z) \left(\frac{v(z)}{v(0)}\right)^2 dz \qquad (47)$$

or Love waves, where $y_1=w(z)/w(0)$ and $iy_3=u(z)/w(0)$, are required in multimode synthesis of theoretical seismograms. For a sequence of homogeneous solid layers, these integrals can be written as

$$I_R = c^2 [r_{\alpha_1} B_1 - D_1]^{-2} \sum I_{(m)} \qquad \text{with m=1, 2,..... n.}$$

The integrals $I_{(m)}$ are given by equations (51) and (53) of (9).

For SH-waves we have:

$$I_L = \begin{cases} \left(\frac{c}{\dot{v}_0}\right)^2 \cdot \sum_{m=1}^{n} I_{(m)} & \text{for the (S – L) case} \\ \left(\frac{c}{\dot{v}_0}\right)^2 \cdot \left(\left(\sum_{m=1}^{n} I_{(m)}\right) + I_{(S-S)}\right) & \text{for the (S – S) case} \end{cases} \qquad (48)$$

with:

$$I_{(m)} = \int_{z_{m-1}}^{z_m} \rho_m \cdot \left(\frac{\dot{v}(z)}{c}\right)^2 dz$$

$$I_{(S-S)} = \int_{z_{n-1}}^{\infty} \rho_n \cdot \left(\frac{\dot{v}(z)}{c}\right)^2 dz \qquad (49)$$

The integrals $I_{(m)}$ can be computed analytically, both for Rayleigh and Love waves (9, 2). For details about the analytic computation of (48) see Appendix B.

I. MODE FOLLOWER AND STRUCTURE MINIMIZATION

Since all the problems connected with the loss of precision at high frequencies have been solved (9) the summation of higher modes of surface waves allows the generation of complete strong motion synthetics even at high frequencies. The key point in the use of multimode summation, both for Love and Rayleigh modes, is an efficient computation of the phase velocity for the different modes at sufficiently small frequency intervals Δf with sufficient precision. To be efficient it is not advisable to determine at each frequency and for each mode the zeros of the dispersion function using the standard root-bracketing and root-refining procedure (8). This must be used only when strictly necessary, as for instance at the beginning of each mode. For all other points i of each mode, the phase velocity can be estimated by cubic extrapolation, using the values of the phase slowness s=1/c and df/ds already determined at frequencies f_{i-2} and f_{i-1}. However, the precision that can be reached in this way is not satisfactory, thus the phase velocity value must be refined. This can be done by an iterative cubic fit in the F-c plane.

Once the problem of an efficient determination of phase velocities is overcome, two other main problems must be solved at each frequency: (a) to correctly follow a mode and (b) to determine the minimum number of layers to be used. The problem of correctly following a mode arises in the high-frequency domain (f>0.1Hz), where several higher modes are very close to each other. The determination of the minimum number of layers to be used - structure minimization - is critical in order to reach a high precision in phase velocity determination spending the minimum possible computer time. In order to ensure high efficiency in the computation of synthetic seismograms, it is necessary to compute the phase velocity, phase attenuation, group velocity, ellipticity, energy integral and eigenfunctions and their maximum depth of penetration at constant frequency intervals. To reach a maximum frequency of 10 Hz, a satisfactory step is 0.05 Hz. To determine the total number of modes present in the frequency interval considered, we fix $c=c_0$ a value close to β_n, where β_n is the S-wave velocity in the half-space, and we increment f to find its values corresponding to zeros of the dispersion function $F(f,c_0)$ (8). Obviously, starting from f=0, the first zero in $F(f,c_0)$ corresponds to the fundamental mode, the second to the first higher mode, and so on. The values of f for which $F(f,c_0) = 0$ are used as starting frequencies (the lowest frequencies) for the computation of the different modes. Once the starting frequency for each mode is defined, it is possible to compute, beginning from the fundamental mode, all dispersion relations. This is accomplished by keeping f fixed and varying c, the procedure being

applied at all of the equally spaced frequency points of the chosen frequency interval.

More details about the mode follower and the complete description of the procedure for structure minimization are given in (11).

8. ATTENUATION DUE TO ANELASTICITY

The treatment of anelasticity requires, for causality reasons, the introduction of body wave dispersion (BWD) (12). In a medium with constant Q, the P- and S-wave phase-velocity can be expressed:

$$A_1(\omega) = \frac{A_1(\omega_0)}{1 + \frac{2}{\pi} \cdot A_1(\omega_0) \cdot A_2(\omega_0) \cdot \ln\left(\frac{\omega_0}{\omega}\right)} \qquad (50)$$

$$B_1(\omega) = \frac{B_1(\omega_0)}{1 + \frac{2}{\pi} \cdot B_1(\omega_0) \cdot B_2(\omega_0) \cdot \ln\left(\frac{\omega_0}{\omega}\right)} \qquad (51)$$

The layer index m is omitted in equations (50) and (51). $A_1(\omega_0)$ and $A_2(\omega_0)$ are the P-wave velocity and the P-wave phase attenuation, while $B_1(\omega_0)$ and $B_2(\omega_0)$ are the S-wave velocity and the S-wave phase attenuation at the reference angular frequency ω_0 (see also 11). The quantities A_1 and A_2 and B_1 and B_2 are related to the complex body-wave velocity α and β (8):

$$\frac{1}{\alpha} = \frac{1}{A_1} - i \cdot A_2 \qquad (52)$$

$$\frac{1}{\beta} = \frac{1}{B_1} - i \cdot B_2 \qquad (53)$$

In the computation we have chosen the reference angular frequency $\omega_0 = 2\pi$ radians. In anelastic media the surface wave phase velocity c must be expressed as a complex quantity:

$$\frac{1}{c} = \frac{1}{C_1} - i \cdot C_2 \qquad (54)$$

C_1 is the attenuated phase velocity and C_2 is the phase attenuation, which is necessary for the computation of seismograms. C_2 can be estimated by using the variational technique (13, 14). The phase attenuation C_2 is given by (1, 2, 11). For Rayleigh waves:

$$C_2 = \left(2\omega I_3 \bar{k}\right)^{-1} / \operatorname{Im}(I_4)$$

where $\bar{k}$ is the wave number in the perfectly elastic case and:

$$I_3 = \int_0^{\infty} \left\{ \left[(\lambda + 2\mu) - \frac{\lambda^2}{(\lambda + 2\mu)} \right] y_3^2 + \frac{1}{k} \cdot \left(y_1 y_4 - \frac{\lambda}{(\lambda + 2\mu)} y_2 y_3 \right) \right\} dz$$

$$I_4 = \int_0^{\infty} \left\{ \delta(\lambda + 2\mu) \left[\frac{1}{(\lambda + 2\mu)^2} \left(y_2^2 + 2k\lambda\, y_2 y_3 \right) + k^2 \left(1 + \frac{\lambda^2}{(\lambda + 2\mu)^2} \right) y_3^2 \right] \right.$$

$$\left. + \delta\mu \frac{1}{\mu^2} y_4^2 - \delta\lambda \left[\frac{2k}{(\lambda + 2\mu)} \left(y_2 y_3 + k\lambda\, y_3^2 \right) \right] \right\} dz$$

and $y_2 = \sigma(z)/w(0)$ and $iy_4 = \tau(z)/w(0)$,

$$\delta\mu = \rho\left(\beta_1^2 - \beta_2^2 - \bar{\beta}^2\right) + 2i\rho\beta_1\beta_2$$

$$\delta\lambda = \rho\left[\left(\alpha_1^2 - \alpha_2^2 - \bar{\alpha}^2\right) - 2\left(\beta_1^2 - \beta_2^2 - \bar{\beta}^2\right)\right] + i\rho 2\left(\alpha_1\alpha_2 - 2\beta_1\beta_2\right)$$

$$\delta(\lambda + 2\mu) = \rho\left(\alpha_1^2 - \alpha_2^2 - \bar{\alpha}^2\right) + i2\rho\alpha_1\alpha_2$$

In these expressions α and β are the compressional and shear-wave velocities in the perfectly elastic case.

For Love waves (2,11):

$$C_2 = \frac{\int_0^{\infty} \mu \cdot B_1 \cdot B_2 \cdot \left(\frac{\sigma_z^2}{\mu^2 \cdot k^2} + v^2 \right) dz}{c \int_0^{\infty} \mu \cdot v^2 dz} \qquad (56)$$

All these integrals can be calculated analytically, since simple analytic expressions are known for the eigenfunctions. The details of the computations of equation (56) are given in Appendix B.

The most important effect of the attenuation is the modification of the wave velocities and the decay of amplitude in the final computations

of seismograms. As the variational technique is only an approximated method, the C_2 values can be in error by as much as 20 per cent in comparison with the exact method. This error arise mainly from the use of the elastic and therefore real eigenfunctions to compute the phase attenuation.

Recently (15) showed the limits of the variational technique in the locked mode approximation, which can be obtained by limiting the model with a rigid or liquid halfspace. He showed, that an error in amplitudes up to 100 per cent can occur, when dealing with low Q-values. The error increases when the Q-values undergo large variations with depth. Introducing a solid halfspace in the model and using the structure minimization procedure prevents this kind of error.

9. RESPONSE TO BURRIED SOURCES

To include the seismic source in the computations, the formulation due to (16) is used. A detailed description of the fault model of an earthquake used in the following computations is given in (5). Accordingly, in the reference system of Figure 1, for the double couple point source, the asymptotic expression of the Fourier time transform of the j-th Love(U_L)- or Rayleigh(U_R^R, U_R^V)-mode displacement at the free surface at a distance r from the source can be written as:

$$U_L = R(\omega) \cdot e^{i\Phi_0} \cdot e^{-\frac{i3\pi}{4}} \cdot k_L^{\frac{1}{2}} \cdot \chi_L(\theta, h) \cdot A_L \cdot \frac{e^{-ik_L r}}{\sqrt{2\pi r}} \cdot e^{-\omega r C_{2_L}} \qquad (57)$$

$$U^R_R = R(\omega) \cdot e^{i\Phi_0} \cdot |n| \cdot e^{-\frac{i3\pi}{4}} \cdot k_R^{\frac{1}{2}} \cdot \varepsilon_0 \cdot \chi_R(\theta, h) \cdot A_R \cdot \frac{e^{-ik_R r}}{\sqrt{2\pi r}} \cdot e^{-\omega r C_{2_R}} \qquad (58)$$

$$U^V_R = e^{-\frac{i\pi}{2}} \cdot \varepsilon_0^{-1} U_R \qquad (59)$$

where $R(\omega)$ is the Fourier transform of the equivalent point-force time function, n is the unit vector perpendicular to the fault and has units of length, Φ_0=arg $R(\omega)$ is the initial phase and ε_0=-u*(0)/w(0) is the ellipticity. The factors A_R A_L are given by:

$$A_L = \frac{1}{2 \cdot c \cdot u \cdot I_{1_L}} \qquad (60)$$

and

$$A_R = \frac{1}{2 \cdot c \cdot u \cdot I_{1_R}} \qquad (61)$$

where c and u are the phase and group velocities for Love and Rayleigh waves respectively.

The effect of anelasticity is expressed by the term:

$$e^{-\omega r C_2} \qquad (62)$$

where C_2, which indicates the phase attenuation either for Love or Rayleigh waves, can be determined as shown in section 8.

$\chi(\theta,h)$ is the azimuthal dependence given by:

$$\chi_R(\theta,h) = d_0 + i \cdot (d_{1_R} \sin\theta + d_{2_R} \cos\theta) + d_{3_R} \sin 2\theta + d_{4_R} \cos 2\theta$$

for P-SV waves, and by

$$\chi_L(\theta,h) = i \cdot (d_{1_L} \sin\theta + d_{2_L} \cos\theta) + d_{3_L} \sin 2\theta + d_{4_L} \cos 2\theta$$

for SH waves.

$$d_0 = \tfrac{1}{2} \cdot B(h) \cdot \sin\lambda \cdot \sin 2\delta$$
$$d_{1_R} = -C(h) \cdot \sin\lambda \cdot \cos 2\delta$$
$$d_{2_R} = -C(h) \cdot \cos\lambda \cdot \cos\delta$$
$$d_{3_R} = A(h) \cdot \cos\lambda \cdot \sin\delta$$
$$d_{4_R} = -\tfrac{1}{2} \cdot A(h) \cdot \sin\lambda \cdot \sin 2\delta$$

$$d_{1_L} = G(h) \cdot \cos\lambda \cdot \cos\delta$$
$$d_{2_L} = -G(h) \cdot \sin\lambda \cdot \cos 2\delta$$
$$d_{3_L} = \tfrac{1}{2} \cdot V(h) \cdot \sin\lambda \cdot \sin 2\delta$$
$$d_{4_L} = V(h) \cdot \cos\lambda \cdot \sin\delta$$

θ is the angle between the strike of the fault and the epicenter-station direction, λ is the rake angle, δ is the dip angle and h is the source depth. The source geometry and the coordinate system associated with the free surface is given in Figure 3. A(h), B(h), C(h), G(h) and V(h) depend on the values of the eigenfunctions at the hypocenter:

$$A(h) = -\frac{u^*(h)}{w_0}$$

$$B(h) = -\left(3 - 4\frac{\beta^2(h)}{\alpha^2(h)}\right)\frac{u^*(h)}{w_0} - \frac{2}{\rho(h)\alpha^2(h)} \cdot \frac{\sigma^*(h)}{\dot{w}_0 / c}$$

$$C(h) = -\frac{1}{\mu(h)} \cdot \frac{\tau(h)}{\dot{w}_0 / c}$$

$$G(h) = -\frac{1}{\mu(h)} \cdot \left(\frac{v^*(h)}{\frac{\dot{v}_0}{c}}\right) = \frac{1}{k \cdot \mu(h)} \cdot \frac{v(h)}{v_0}$$

$$V(h) = \frac{\dot{v}_s(h)}{\dot{v}_0} = \frac{v_s(h)}{v_0}$$

The asymptotic expressions (57), (58) and (59) allow the computation of synthetic seismograms with at least 3 significant figures as long as kr>10 (5) and is equivalent to the expression in terms of the seismic moment [e.g. see equations (7.148), (7.149) and (7.150) in (14)].The seismogram related to a given mode is obtained by the inverse Fourier transform of (57), (58) and (59).

The extension of these results to the available formalism for sources with finite dimensions and durations is quite straightforward; the necessary details can be found in (11).

10. TWO DIMENSIONAL MODELS

The expressions (57), (58) and (59), describing the displacement due to surface-wave modes, have been generalized to the case of two stratified quarterspaces in welded contact (17), (3). For example the radial component of displacement spectrum can be written:

$$U = R(\omega) \cdot e^{-i(3\pi/4)} \cdot e^{-i\omega(1/c + 1'/c')} \cdot e^{-(\omega C_2 + 1' C'_2)}$$
$$\frac{1}{\sqrt{J}} \cdot \sqrt{\frac{\omega}{2\pi}} \cdot \frac{\varepsilon'}{\sqrt{2cuI_1}_R} \cdot \Gamma_{ii'} \cdot \sqrt{\frac{\cos\varphi}{\cos\varphi'}} \cdot \frac{\chi_R(\theta,h)}{\sqrt{2c^2 u I_1}_R} \qquad (63)$$

It is assumed that the source and the receiver are situated far from the sharp vertical discontinuity in comparison to the biggest wavelength of

interest. Equation (63) represents the radial displacement carried by the n-th Rayleigh mode generated by a point source at M(r, l) of a medium j, then transmitted through the boundary between j and j' and recorded at point M'(r', l') on the surface of medium j' as mode n'. As it is evident from Figure 4, r and r' are respectively the distances of source and receiver from the vertical interface, l and l' are the paths travelled by incident and generated waves, ϕ and ϕ' are the angles of incidence and refraction. In eq.(63) the primed quantities refer to the medium where the receiver is placed while the unprimed quantities refer to the medium containing the source. $R(\omega)$ is the Fourier transform of the time function relative to the source, c and c' are the phase velocities, u and u' the group velocities, I and I' are energy integrals ε' is the Rayleigh mode ellipticity of the receiver's medium, $\chi_R(\theta,h)$ is the radiation pattern evaluated for the medium containing the source, $J=(\cos\phi\cos\phi'/c)[(rc/\cos^3\phi)+(r'c'/\cos^3\phi')]$ describes the geometrical spreading of the surface wave energy. The effect of anelasticity is expressed by $e^{-\omega(lC_2+l'C'_2)}$ where C_2 and C'_2 are the phase attenuations in the two media (for more details see (1)).

The coupling coefficients $\Gamma_{jj'}(\omega, \phi, \phi', n, n')$, necessary to describe reflection and transmission phenomena at the boundary, will be discussed in the next section.

10.1. COUPLING COEFFICIENTS

The problem of reflection and transmission of surface waves through lateral discontinuities existing inside the earth can not be solved in an analytical way. Several methods based on different approximations have been proposed to define and estimate surface waves reflection and transmission coefficients. Here only the transmission problem will be discussed, but the same procedure can be adopted to describe the reflection problem.

The approximations suggested by (18) were chosen to evaluate a set of coupling coefficients that gives a picture of how the energy carried by the normal modes, characteristic of the medium with the source, and transmitted through the discontinuity, is redistributed among the normal modes, of the medium with the receiver.

The starting point is the stress-displacement system of the incoming surface wave mode. Decomposing the incident wave into the P-component and the SV-component, we turn to a solvable problem of reflection and transmission of P-SV waves. Referring to Figure 5, the problem will be solved for every single section on the vertical interface as if it would be infinite, using well known formulae based on Snell's law and continuity conditions of displacement and traction at the boundary. Since the sections are in reality limited, in this way we neglect the effects arising at the corners between the horizontal interfaces and the vertical one. We can think the corner effects as giving rise to a system of diffracted waves. These arise because it is impossible to satisfy exactly the continuity conditions also on the horizontal interfaces. With this approximation a reflected and a transmitted stress-displacement system can be determined. They contain a P-component and an SV-component but their combination does not give a Rayleigh wave any longer because the continuity conditions at the horizontal boundaries are not matched. The medium with the receiver is characterized by a set of normal modes corresponding to solutions of the wave equation verifying the continuity conditions on the horizontal interfaces. Our aim is to determine how each of these modes is excited by the modes contained in the incident wave, or in other words, how the transmitted system redistributes among the normal modes existing in medium with the receiver. To obtain this, the transmitted system is projected on the system of normal modes characteristic of the medium with the receiver using an appropriate definition of scalar product.

A stress-displacement vector for an incident wave identified by the subscript I can be defined

$$A_I = (u_I, v_I, w_I, p_{xxI}, p_{xyI}, p_{xzI}) \qquad (64)$$

where p_{ij} is the j-th component of the stress acting across the plane normal to the i-th axis. The p_{xj} (with j = x, y, z) stress components are considered because for the geometry of the problem only stresses acting on the vertical plane x=0 are involved. Defining similarly a stress-displacement vector relative to the normal modes system of the medium with the receiver, the projection of vector A_I on the vector A_{II} is performed via a scalar product, suggested by Herrera's orthogonality relation (19):

$$\langle A_I, A_{II} \rangle = \frac{1}{2i} \int_0^{\infty} [u_I \bar{p}_{xxII} + v_I \bar{p}_{xyII} + w_I \bar{p}_{xzII} - p_{xxI} \bar{u}_{II} - p_{xyI} \bar{v}_{II} - p_{xzI} \bar{w}_{II}] dz \qquad (65)$$

the bar denotes complex conjugate. Indicating the transmitted system by the vector

$$A_T = (u_T, v_T, w_T, p_{xxT}, p_{xyT}, p_{xzT}) \tag{66}$$

the quantity:

$$\gamma_{jj'}^{(m,m')} = \frac{\left\langle A_T^{(m)}, A_{II}^{(m')} \right\rangle}{\left\langle A_I^{(m)}, A_I^{(m)} \right\rangle^{\frac{1}{2}} \left\langle A_{II}^{(m')}, A_{II}^{(m')} \right\rangle^{\frac{1}{2}}} \tag{67}$$

provides the amplitude of mode n' of A_{II} due to mode n of A_I, contained in the transmitted vector A_T. If the amplitude of a wave generated by an incident wave of unit amplitude is preferred:

$$\Gamma_{jj'} = \gamma_{jj'}^{(m,m')} \frac{\left\langle A_I^{(m)}, A_I^{(m)} \right\rangle^{\frac{1}{2}}}{\left\langle A_{II}^{(m')}, A_{II}^{(m')} \right\rangle^{\frac{1}{2}}} = \frac{\left\langle A_T^{(m)}, A_{II}^{(m')} \right\rangle}{\left\langle A_{II}^{(m')}, A_{II}^{(m')} \right\rangle} \tag{68}$$

$\Gamma_{jj'}$ is the coupling coefficient appearing in equation (63).

The approximations used to obtain $\Gamma_{jj'}$ are:

a) the Rayleigh modes for the two media are evaluated assuming each medium as a halfspace instead of a quarterspace; this is a reasonable assumption a few wavelengths from the interface;

b) a system of diffracted waves arising at the corners of the sections is neglected; this is a good approximation for a small contrast in the elastic parameters characterizing the two quarterspaces (18).

The crucial approximation is contained in this last point. Although it is not easy to estimate quantitatively the accuracy of it, a criterion is given by a reversibility theorem that is demonstrated in section 10.3.

10.2. THE COUPLING INTEGRAL

To calculate $\langle A_T, A_{II} \rangle$ and $\langle A_{II}, A_{II} \rangle$, once the explicit expressions for the various displacement and stress components are assigned, the integration indicated in equation (65) must be performed over the semiaxis z>0. At this stage we limit our analysis to the 2-dimensional case of the x-z plane, to the Rayleigh modes and to normal incidence. These three assumptions are strictly connected because for non-normal incidence as for the 3-dimensional case there is transmission of P and SV into SH energy, so conversion between Rayleigh and Love modes must be taken into account. The development of the pertinent algorithms and related codes is presently in progress at ICTP-ICE-IGG. The integral (65) simplifies in the following way:

$$\left\langle A_T, A_{II} \right\rangle = \frac{1}{2i} \int_0^\infty [u_T \bar{p}_{xxII} + v_T \bar{p}_{xxII} - p_{xxT} \bar{u}_{II} - p_{xzT} \bar{w}_{II}] dz \tag{69}$$

Bearing in mind that the z-dependence is different in various layers, the integral (69) may be evaluated as a sum of integrals over each section. As it can be seen from Figure 5:

$$\int_0^\infty dz \rightarrow \sum_{s=0}^{S-1} \int_{H_s}^{H_{s+1}} dz + \int_{H_S}^{\infty} dz$$

where H_S is the depth of the s-th section.

These integrals can be computed both numerically and analytically. In the numerical integration the eigenfunctions are sampled with a constant step (for frequencies up to 1 Hz the step used is 250 m) down to the halfspace, where displacements and stresses tend to zero, and of course the integration along z cannot be performed to infinity but to some arbitrary large depth. To treat frequencies higher than 1 Hz one has to reduce the eigenfunctions sampling step to follow correctly the number of oscillations per cycle. Therefore increasing frequency causes the numerical integration to become more and more time consuming along with the limited precision introduced by the approximated integration in the halfspace. These problems of computation time and precision can be overcome by the analytic integration.

Developing the cross-products between stresses and displacements in equation (69), separately for the transmitted P and SV waves, it can be seen that the integrals we end up with are of an elementary type, involving sinusoidal and hyperbolic functions. The difficulty consists in handling correctly the different situations existing in each section, according to the values of the phase velocities c compared to α and β in the two media.

Let's refer again to the structure displayed in Figure 5, where the superscripts 1, 2 refer respectively to medium 1 and medium 2. On the left

side the functions for stresses and displacements are denoted by f(z) and the various parameters with $\alpha^{(1)}_{(z)}, \beta^{(1)}_{(z)}$ while on the right side g(z), $\alpha^{(2)}_{(z)}$, $\beta^{(2)}_{(z)}$ are used.

For $H_S<z<H_{S+1}$, $f(z)=f_i(z-H_S)$, $\alpha^{(1)}_{(z)}=\alpha^{(1)}_i$

For $H_{S-1}<z<H_S$, $g(z)=g_{j-1}(z-H_{S-1})$, $\alpha^{(2)}_{(z)}=\alpha^{(2)}_j$

The integrals involved will be of the type:

$$J_{s+1}=\int_{H_s}^{H_{s+1}} dz\left[g_j(z-H_{s-1})\, f_i(z-H_s)\right] \qquad (70)$$

The behaviour of the functions f and g, depending on the values of the phase velocity c with respect to $\alpha^{(1)}, \beta^{(1)}, \alpha^{(2)}, \beta^{(1)}$, can be either oscillatory or exponential (see also sections 3 and 4).

The general expression (70) can be simplified if in the starting model some fictitious interfaces are introduced so that the layering in the two structures is the same (see Figure 6). In the new m-th layer the elastic parameters maintain the same value, while the layer constants (e.g. A_m, B_m, C_m, D_m for Rayleigh waves) and the arguments of f and g change according to the new value of H_m (Figure 6). This occurs because a new interface, though artificial, imposes the introduction of new continuity conditions. In this way any structure can be rearranged to a new one where the layers are lined up. For this last case, as it can be easily verified, the integrals required are simpler, and have the form:

$$J_m=\int_{H_m}^{H_{m+1}} dz\,[g_m(z-H_m)\, f_m(z-H_m)]=\int_0^{h_m} dz[f_m(z)g_m(z)] \qquad (71)$$

where $h_m = H_{m+1} - H_m$. The integral depends only on the thickness of the section, not on its depth.

The case in which one or both the final sections are a halfspace is characterized by an exponential decay of stresses and displacements at increasing z. In the situation of halfspace $\alpha_s > \beta_s > c$ and consequently $A_S=B_S$, $C_S=D_S=1$, the integrals to be evaluated have the form

$$\int_{H_{S-1}}^{H_S} dz\left[e^{-\gamma^{(1)}(z-H_{S-1})} g_S(z-H_{S-1})\right]=\int_0^{h_S} dz\left[e^{-\gamma^{(1)}z} g_S(z)\right]$$

$$\int_{H_S}^{\infty} dz\left[e^{-\gamma^{(1)}(z-H_{S-1})} e^{-\gamma^{(2)}(z-H_S)}\right]=\int_0^{\infty} dz\left[e^{-\gamma^{(1)}z}\, e^{-\gamma^{(2)}(z-h_S)}\right]$$

where $h_S = H_S - H_{S-1}$. The situation is represented in Figure 7 where, for medium 1 (l=1,2), $\gamma^{(l)}=k^{(l)}\, r^*_\alpha{}^{(l)}$ for P-waves and $\gamma^{(l)}=k^{(l)}\, r^*_\beta{}^{(l)}$ for SV waves. A complete list of the various integrals is given in Appendix B of (3).

10.3 NORMALIZATION PROPERTIES AND REVERSIBILITY THEOREM

The general scheme to study the dynamics of continuous media is provided by the Lagrangian formulation. In this frame, using variational techniques and Hamilton's principle, it is possible to give a physical meaning to the integral appearing in equation (65). In the case of Rayleigh waves propagating in the x-direction the displacement assumes the expression

$$u(x, z, t) = e^{-i(\omega t - kx)}[u(z)\,;0;iw(z)] \qquad 0 \le z < \infty \qquad (74)$$

Looking at the normalization integral of equation (3):

$$J_m = \frac{1}{2i}\int_0^{\infty}[\,u_m(z)\,\bar{p}_{xz}(k_m, z) + iw_m\,\bar{p}_{xz}(k_m, z)$$

$$- p_{xz}(k_m, z)\,u_m - ip_{xz}(k_m, z)w_m(z)\,]\,dz \qquad (75)$$

it can be demonstrated that

$$J_m = \frac{(UE)_m}{\omega} = \frac{1}{\omega}\psi_m \qquad (76)$$

where ψ_m is proportional to the energy transmitted per unit time across an infinite stripe of unit width in the y-z plane. Thus it is convenient to normalize the surface waves system in such a way that, for each mode n, the energy crossing per unit time an infinite stripe in the y-z plane is equal to 1. This can be obtained passing from

$$(u_m, w_m) \quad \text{to} \quad \left(\frac{u_m}{\sqrt{\omega J_m}}, \frac{w_m}{\sqrt{\omega J_m}}\right) \qquad (77)$$

Furthermore, since the main part of the surface displacement can be represented as a superposition of modes

$$u(x, z, t) = \sum_m a_m e^{-i(\omega t - k_m x)} [u_m(z); O; i w_m(z)] \tag{78}$$

the normalization implies that the energy transmitted per unit time across the stripe is given by

$$UE = \sum_m |a_m|^2$$

For a layered structure with a vertical interface along the z-axis (fig.1), with our approximations, the displacement on the left of the interface (medium 1) is given by the superposition of N modes

$$u(x, z, t) = \sum_{m=1}^{N} e^{-i\omega t} \left[a_m e^{-ik_m x} + b_m e^{ik_m x} \right] (u_m; O; i w_m) \qquad x < O \tag{79}$$

Similarly in the right side medium (medium 2) the displacement

$$u(x, z, t) = \sum_{m'=1}^{N'} e^{-i\omega t} \left[a_{N+m'} e^{-ik_{m'} x} + b_{N+m'} e^{ik_{m'} x} \right] (r_m; O; i s_m) \qquad x > O \tag{80}$$

is given by the superposition of N' modes. The quantities a_i, i=1,2...N+N' are the complex amplitudes of the incoming normal modes; the quantities b_j, j=1,2...N+N' are the complex amplitudes of the outgoing, reflected or transmitted, normal modes. The linearity of equations of motion establishes a linear relation between the two sets of amplitudes. Indicating with $\mathbf{a}=(a_1,\ldots,a_{N+N'})$, $\mathbf{b}=(b_1,\ldots b_{N+N'})$ the two vectors of N+N' components there is a matrix S such that

$$\mathbf{b} = S\mathbf{a} \tag{81}$$

The elements of the scattering matrix S correspond to the reflection and transmission coefficients of the problem studied. From equation (76) it follows that the energy incident per unit time on the discontinuity surface is given by:

$$(UE)_{inc} = \sum_m |a_m|^2 = \mathbf{a} \cdot \bar{\mathbf{a}} \tag{82}$$

The outcoming energy, transmitted or reflected into the different modes, is

$$(UE)_{out} = \sum_m |b_m|^2 = \mathbf{b} \cdot \bar{\mathbf{b}} \tag{83}$$

Since the total energy leaving the vertical boundary is equal to the incident one, S is a unitary matrix, i.e.

$$S S^{+} = 1 \qquad S_{ij} \bar{S}_{kj} = \delta_{ik} \tag{84}$$

When the scattering into body waves is neglected, as we do here, S is not any more a unit matrix and the relevance of the approximation can be estimated by the difference between S and the unit matrix.

Another property of the S matrix follows from the fact that the equations of motion are invariant for complex conjugation and time inversion. This means that if $u(x,z,t)$ is a solution, also $\bar{u}(x, z, -t)$ is a solution. The linear relation given by equation (81) changes to:

$$\bar{\mathbf{a}} = S\bar{\mathbf{b}} = S S \bar{\mathbf{a}} \tag{85}$$

so that

$$S S = 1 \qquad S_{ij} \bar{S}_{jk} = \delta_{ik} \tag{86}$$

The matrix S is then symmetric, $S_{ij} = S_{ji}$, S_{ij} being the amplitude transmission or reflection coefficient from the mode j into the mode i ($b_i = S_{ij} a_j$). According to the mode normalization given in equation (77), the energy crossing per unit time a given surface is equal to 1. Consequently, S_{ij}^2 corresponds to the energy transmitted (or reflected) from mode j to mode i; from this it follows the reversibility property expressed by the relation

$$S_{ij}^2 = S_{ji}^2 \tag{87}$$

An example of the exchanges of energy between two modes of two fferent media in welded contact is given in Figure 8, and shows, for the ructural models under consideration (see Figure 9), the degree of validity assumption (b) of section 10.1. In this Figure, like in the following ones, e first two characters of each acronym refer to the incident mode, the last io to the outgoing one. For example, the coupling between the second gher mode of structure C (incident mode) and the fundamental mode of ructure P (outgoing mode) would be indicated as C2PF. Two further :amples, shown in Figure 10a and Figure 10b, allow to appreciate how the coming energy related to one mode redistributes within the outgoing odes. When the incident fundamental mode is considered (Fiugure 10a), most all of the energy is transmitted into the outgoing fundamental one :FPF). Looking at the sum of the outgoing energies (thin solid line), it can be en that in the whole frequency range it is enough to consider just three itgoing modes to transmit across the boundary more than 90% of the coming energy. This is no longer true when the first higher mode is cident (Figure 10b).

I. EXAMPLES OF COMPUTATION

I.1 FREQUENCY DOMAIN

The layered velocity model in Figure 11 and Table 1 is used as an :ample. It represents an average structure of the Friuli seismic area in the outhern pre-Alps, close to the May 6, 1976, Friuli earthquake.

I.1.1. Phase velocities

The Rayleigh wave dispersion curves for the first 154 modes are iown in Figure 12a. The modes are well separated for phase velocities less an about 3.35 km/s, which corresponds to the S-wave velocity in the pper part of the upper crustal low-velocity channel. For higher phase elocities, the dispersion curves are closely packed together. Ther first irves correspond to waves that sample only the first few kilometers of the ust, while the latter ones correspond to waves that sample the entire ructure. Essentially three "quasi-osculation" types can be recognized (see igure 12b). The first corresponds to horizontal "quasi-osculations" around a onstant phase velocity (e.g. 4.25 and 3.50 km/s) and are related to the ructural layering. The second is the standard sequence of channel and crustal waves (20) due to the presence of a low velocity layer. The presence of two low-velocity layers is clearly recognizable in the range of phase velocities between 3.35-3.45 km/s and 3.75-3.85 km/s. The third is made up of very steep "quasi-osculations" and corresponds to a family of waves mainly sampling the wave guide formed by the sedimentary layers.

The dispersion curves for the first 153 Love modes are shown in Figure 13a. For S-wave velocities less than 3.35 km/s the modes are well separated. This velocity corresponds to the S-wave velocity in the upper part of the crustal low-velocity zone (LVZ). Modes situated in the part of the spectrum below this phase velocity value sample therefore the part of the crust above the uppermost LVZ. In the part of the spectrum with higher phase velocities the dispersion curves are packed together. An enlarged portion of this part is presented in Figure 13b. Since two LVZ are present in the structural model, areas are seen where the higher Love wave modes decompose into families of low-velocity channel waves and families of waves propagating in the upper crust. A member of the family of upper-crustal waves can be identified at a frequency of about 4 Hz in the phase velocity range 3.35-3.45 km/s. Another type of apparent continuity of the phase velocities for adjacent modes can be related to the structural layering (for example at a phase velocity of about 4.25 km/s). Such parts of the spectrum represent refracted waves at strong elastic impedance contrasts. They are characterized by phase velocities which tend to become constant with increasing frequency.

11.1.2.Group velocities

The group velocities for Rayleigh waves are shown in Figure 14a,b,c. The diagram has been divided into three parts due to the complexity of the pattern. Although it is difficult to follow an individual mode, it is relatively easy to follow the behavior of channel and crustal waves as well as that of the sedimentary waves. The stationary phases with group velocity between 0.3 and 1.6 km/s, visible for frequencies greater than about 3 Hz, correspond to waves essentially propagating in the low-velocity sediments. For group velocities around 2.4-2.8 km/s, stationary phases are visible at frequencies greater than 5 Hz; these phases can be associated with waves propagating near the bottom of the sediments. The stationary phases, formed by the combination of several higher modes visible in the group velocity interval of 3.0-3.3 km/s, starting from frequencies on the order of 3 Hz, can be considered the high frequency equivalent of Li and Lg phases (21,

22, 23, 24). For frequencies larger than 1 Hz, two flat envelopes corresponding to the two-channel velocities can be easily seen at about 3.75 and 3.35 km/s. Near 3 Hz an envelope of group velocities as low as 1.6 km/s is clearly seen. This corresponds to the waves sampling the sedimentary layers wave guide.

The group velocity spectrum for Love waves is presented in Figure 15a,b. It has been divided into two parts due to the complexity of the pattern. Modes with group velocities less than about 2.8 km/s correspond to waves propagating in the low-velocity sediments. In the part of the spectrum, where group velocities are in the interval 2.8-3.2 km/s, several higher modes form stationary phases. They correspond to families of waves propagating in the upper crust and are characterized by the same type of mode-to-mode continuation as in the phase velocity curves. They can be interpreted as the high-frequency equivalent of Lg phases (21, 22, 23, 24), which are propagating in the upper part of the continental crust. The flat portions of group velocity curves formed by a large number of higher modes at about 3.35 km/s and 3.75 km/s correspond to waves propagating in the upper and lower channel.

11.1.3.Energy integral

The energy integral can serve as an estimate of the contribution of the different modes to the surface displacement. In general, neglecting the influence of the source depth on the excitation of different modes, small values of the energy integral I_1 correspond to large surface displacements. For Rayleigh (Figure 16) waves it is interesting to observe that for frequencies smaller than 3 Hz the fundamental mode dominates, while around 3 Hz several higher modes are characterized by small values of I_1. These modes mainly sample the sediments. In the frequency range between 3-6 Hz, the first higher mode is dominant, while for larger frequencies the fundamental mode again dominates the surface displacement. A common feature to all figures are the very narrow peaks around 3 Hz associated with the presence of sediments. If the source is located near the sedimentary layers, one may expect significant surface motion mainly in the horizontal component even if I_1 is quite large. In these portions of the spectrum, the eigenfuntions are characterized by large lobes concentrated in the sedimentary layers, and the ellipticity (see section 11.1.4) becomes very large. Also, the fundamental mode is not dominant, i.e., it does not have the smallest I_1, over the entire spectrum due to the sedimentary layers.

For Love waves, on the contrary, in the whole frequency range, the fundamental mode has the lowest values of I_1 (Figure 17). For a shallow source, the fundamental mode generally dominates the surface displacement. The mode-to-mode continuations in the lower part of the energy integral curves correspond to the high frequency equivalent to Lg waves. The low values of the energy integral indicates that this waves can give rise to significant amplitudes at the surface. Most of the energy of channel waves is concentrated in the channel. Therefore, the energy integral of these families takes higher values then that for upper-crustal waves. For a given member of this family the maximum displacement in the low-velocity zone becomes larger relative to the displacement at the free surface, with increasing frequency. Therefore, the energy integral of this member is characterized by increasing values with increasing frequency. This can be seen in the general pattern of the upper part of Figure 17.

11.1.4. Ellipticity

Another important quantity describing Rayleigh-mode particle motion is the ellipticity $\epsilon_0=-u^*(0)/w(0)$, i.e., the ratio between the horizontal and vertical components of motion at the free surface. It is very important to observe that ϵ_0 has abrupt discontinuities. More precisely, at some frequencies $\epsilon_0 \rightarrow \pm \infty$ as a consequence of the fact that w(0) passes through zero. This is not an obvious property, and it strongly depends upon the elastic properties of the layers closest to the free surface. For frequencies not exceeding 1 Hz and for Earth models without sedimentary layers, these discontinuities are present only once in a given mode and only for modes with large-order number (1). However, when there are sediments at the top of the model, several discontinuities are also present in each of the first higher modes (Figure 18). Thus, due to the presence of sediments, the particle motion of several modes is essentially horizontal over a quite wide frequency range.

11.1.5. Quality factor Q_X

The phase attenuation C_2 is related to the quality factor Q_X by the relation

$$1/Q_X = 2\, C_1\, C_2$$

where C_1 is the anelastic phase velocity (25, 26). For Rayleigh waves the quality factor is presented in Figure 19, while for Love waves in Figure 20. It is practically impossible to follow individual modes in their entirety, yet it is relatively easy to see the effect of the layering in Q_α and Q_β. For instance, the fundamental mode shows a large peak around 0.5 Hz and this corresponds to wave propagation in the crust outside the low-velocity layers where Q_β=400. For frequencies larger than 3 Hz, several modes are characterized by very low values and this indicates wave propagation in the upper sedimetary layers where Q_β does not exceed 100. The trapping in the low-velocity layers, characterized by Q_β=100 and Q_β=50, is clearly visible for several nearby modes that have almost constant Q_x close to 50, 65, and 100. The value 65 represents the weighted average by layer thickness of the values 50 and 100, both present in the upper crustal low velocity zone. Q_β is very low in the sedimentary layers. Modes mainly propagating in these layers are therefore characterized by low Q_x values (e.g. see Figure 20a for Love modes). This is the case for the first few modes, especially for the fundamental and first higher mode. The effect of layering of Q_β can be observed for several nearby modes that have almost constant Q_x, for example Q_x close to 65. The resulting Q_x values are close to the values Q_β of the structural model for those Love wave modes, whose eigenfunction mainly sample the corresponding part of the structure.

11.1.6 Two dimensional case

To compare our results with the ones obtained by other authors, the coupling coefficients have been computed for two lithospheric models (Figure 9), whose elastic properties were proposed by (27) and used by (17). The coupling coefficients obtained by (17), applying the method proposed by (28) to the fundamental modes of the two structures are shown as heavy lines in Figure 21, while thin lines represent the results obtained by (3). As one can see, in the common frequency range the agreement is very good. For each direction of propagation two thin lines are drawn: the upper one has been computed by simply projecting the stress-displacement system of the first medium on the normal mode system of the second one, without taking into account the local effects introduced by the vertical boundary. This represents a possible simplification of the method and of course has the advantage of requiring less computation time. In this example, the results do not differ very much, and it seems that the coupling between the modes is highly dependent on the difference between the eigenfunctions of the two

systems, and that the refraction at the vertical boundary plays just a secondary role. This may be no longer true for models where the contrast between the elastic parameters of the two structures is very strong, and for different angles of incidence.

11.2. TIME DOMAIN

11.2.1. One-dimensional case

The first example corresponds to the November 4, 1976 Brawley, California earthquake. The structural model and source parameters have been proposed by (29). The structure is given in Table 2. Since (30) computed synthetic seismograms for this event with the mode-summation technique limited to the perfectly elastic case, their result provides a useful test, even if limited to the perfectly elastic case, for our programs. Therefore, the source parameters used in the synthesis are the same as those given by (30).

A strike-slip point source is placed on a vertical plane at 6.9 km depth. The rupture velocity time-function is a symmetrical triangle with a base of 1.5 seconds. The rupture velocity time-function is given by $(i/\omega)\cdot R(\omega)$, where $R(\omega)$ is the Fourier transform of the equivalent point-force time-function. At a distance of 33 km from the source, the displacement consists almost entirely of the fundamental mode and the first higher modes (Figure 22). The transverse component of the recorded displacements at the station IVC, 33 km from the source is given in the same figure. The upper frequency limit is 1 Hz. It can be seen that there is generally a very good agreement between the two synthetic signals. There is only a slight difference in the value of the peak amplitudes and in the coda, due to the effect of attenuation included in our codes. Similar examples for radial and vertical component of motion are given by (11).

In the second example we present synthetic seismograms for the structural model FRIUL7A shown in Table 1. The upper frequency limit is 10 Hz. The source parameters correspond to the Friuli, May 6, 1976 earthquake in the point source approximation, with the source parameters taken from (31). The receivers are chosen in the direction of the dominant lobe of the radiation pattern of SH-waves (north-east direction, with a strike-receiver angle of 235°), resulting from the selected source parameters. Synthetic ground displacements, velocities and accelerations are presented in the lower part of Figure 23. The signals are filtered with a Gaussian filter (the first filtered frequency is at 9 Hz and the reduction of the amplitude by

factor 1/100 at the cutoff frequency of 10 Hz). This filter prevents ringing due to the cutoff frequency. A decomposition of the displacement into different sets of modes is presented in the upper part of the figure. It shows that the higher modes are essential in defining the shape of the waveform, especially in the body wave part of the synthetic seismograms. In Figure 24a transverse component synthetics due to a source with a finite rise time are presented. The rupture velocity time-function is a symmetrical triangle with a base of 0.5 seconds. The signals are filtered with the already described Gaussian filter. As expected, the energy is shifted to lower frequencies, as the duration of the source is increased. The strong phases at about 35 s, for the signal at 100 km distance from the source (lowest trace), can be identified as the Lg phases. In Figure 24b an example of the radial component is given.

11.2.2. Two dimensional case

Synthetic displacements have been computed putting an instantaneous point-source, corresponding to a double-couple, in one medium and a receiver in the other one, according to the scheme of Figure 25. Both the source and the receiver are 50 km away from the vertical boundary, and the parameters defining the source are as follows: depth 10 km, strike-receiver angle 60°, dip 90°, rake 0°. For each model the fundamental and the first two higher modes have been considered, and the contribution of each incident mode to all of the outgoing modes have been computed. The coupling coefficients for both propagation directions are represented in Figure 26, while the seismograms - vertical (V) and radial (R) components - are shown in Figure 27. In each frame, from top to bottom, the displacements due to the nine possible combinations between the three modes of each model and their sum are plotted. Each seismogram is normalized to the peak value of the sum, and this allows to fully appreciate the relevance of the energy exchanges between modes of different order number. The synthetic seismograms of Figure 27, when compared with the seismograms computed for the two models separately (Figure 28), clearly show the effects of the lateral discontinuity.

The application of the reversibility theorem gives the possibility of evaluating the reliability of the results, even when very complicated models, with high contrasts in the elastic parameters, are in welded contact. Although no comparison with experimental seismograms has been tried yet, the results obtained in the present work encourage us to extend the

frequency limits and to take into account the contact of more than two structures.

The analytical integration proved to be accurate and extremely time-saving (up to 80% faster than the numerical integration, when the eigenfunctions sample the model to the maximum depth).

Appendix A: Derivatives of the matrices for the computation of the group velocities

Three cases have to be distinguished: $c>\beta_m$, $c<\beta_m$ and $c=\beta_m$.

To avoid too heavy notations, layer indexes m and n are dropped. The S-wave velocity is denoted by ß. Introducing body wave dispersion, we have:

$$\beta = \frac{B_1(\omega_0)}{1+\frac{2}{\pi}\cdot B_1(\omega_0)\cdot B_2(\omega_0)\cdot \ln\left(\frac{\omega_0}{\omega}\right)}$$

$B_1(\omega_0)$ and $B_2(\omega_0)$ are the phase velocity and the phase attenuation at the reference angular frequency ω_0. The rigidity is $\mu=\rho\beta^2$, ρ is the density and d is the thickness. Derivatives with respect to c are denoted using a dot symbol ($\dot{}$), while those with respect to ω are denoted with a prime symbol ($'$).

If the halfspace is solid, we use the quantity s (Schwab and Knopoff, 1972):

$$s = -\mu\cdot\left(1-\left(\frac{c}{\beta}\right)^2\right)^{1/2}$$

$$\dot{s} = \frac{\delta s}{\delta c} = \frac{\mu\cdot c}{\beta^2\cdot\left(1-\left(\frac{c}{\beta}\right)^2\right)^{1/2}}$$

$$s' = \frac{\delta s}{\delta\omega} = \frac{2\cdot s\cdot B_2(\omega_0)\cdot\beta}{\pi\cdot\omega}\cdot\left(2+\frac{c^2}{\beta^2-c^2}\right)$$

First case : $c>\beta$

We use here the following notations :

$$r = \left(\left(\frac{c}{\beta}\right)^2-1\right)^{1/2}$$

$$Q = \omega\cdot r\cdot\frac{d}{c} = k\cdot r\cdot d$$

The layer matrix is :

$$b_{ij} = \begin{bmatrix} \cos Q & \frac{\sin Q}{\mu\cdot r} \\ \mu\cdot r\cdot\sin Q & \cos Q \end{bmatrix}$$

We have:

$$\dot{b}_{11} = -\frac{Q\cdot\beta^2\cdot\sin Q}{c\cdot\left(c^2-\beta^2\right)}$$

$$\dot{b}_{12} = \frac{1}{\mu}\cdot\left(-\frac{c\cdot\sin Q}{\beta^2\cdot r^3}+\frac{Q\cdot\beta^2\cdot\cos Q}{c\cdot r\cdot\left(c^2-\beta^2\right)}\right)$$

$$\dot{b}_{21} = \mu\cdot\left(\frac{c\cdot\sin Q}{\beta^2\cdot r}+\frac{Q\cdot\beta^2\cdot r\cdot\cos Q}{c\cdot\left(c^2-\beta^2\right)}\right)$$

$$b'_{11} = -d\left(\frac{r}{c}-\frac{2\cdot B_2(\omega_0)\cdot c}{\pi\cdot\beta\cdot r}\right)\sin Q$$

$$b'_{12} = \frac{d}{\mu\cdot r}\left(\frac{r}{c}-\frac{2\cdot B_2(\omega_0)\cdot c}{\pi\cdot\beta\cdot r}\right)\cos Q-\frac{2\cdot B_2(\omega_0)}{\pi\cdot\beta\cdot r\cdot\rho\cdot\omega}\left(2-\frac{c^2}{\beta^2\cdot r^2}\right)\sin Q$$

$$b'_{21} = \mu\cdot r\cdot d\left(\frac{r}{c}-\frac{2\cdot B_2(\omega_0)\cdot c}{\pi\cdot\beta\cdot r}\right)\cos Q+\frac{2\cdot B_2(\omega_0)\cdot\mu\cdot\beta\cdot r}{\pi\cdot\omega}\left(2-\frac{c^2}{\beta^2\cdot r^2}\right)\sin Q$$

Second case : $c<\beta$

we use here the following notations :

$$r = -i\cdot\left(1-\left(\frac{c}{\beta}\right)^2\right)^{1/2} \qquad \text{with } r = i\cdot r^*$$

$$Q = \omega\cdot r\cdot\frac{d}{c} = k\cdot r\cdot d \qquad \text{with } Q = i\cdot Q^*$$

$$Q^* = \omega\cdot r^*\cdot\frac{d}{c}$$

subsequently:

$$\sin Q = i \cdot \sinh Q^*$$
$$\cos Q = i \cdot \cosh Q^*$$

The layer matrix is :

$$b_{ij} = \begin{bmatrix} \cosh Q^* & \frac{\sinh Q^*}{\mu \cdot r^*} \\ -\mu \cdot r^* \cdot \sinh Q^* & \cosh Q^* \end{bmatrix}$$

We have:

$$\dot{b}_{11} = \frac{Q^* \cdot \beta^2 \cdot \sinh Q^*}{c \cdot (c^2 - \beta^2)}$$

$$\dot{b}_{12} = \frac{1}{\mu} \cdot \left(\frac{c \cdot \sinh Q^*}{\beta^2 \cdot r^{*3}} + \frac{Q^* \cdot \beta^2 \cdot \cosh Q^*}{c \cdot r^* \cdot (c^2 - \beta^2)} \right)$$

$$\dot{b}_{21} = \mu \cdot \left(\frac{c \cdot \sinh Q^*}{\beta^2 \cdot r^*} - \frac{Q^* \cdot \beta^2 \cdot r^* \cdot \cosh Q^*}{c \cdot (c^2 - \beta^2)} \right)$$

$$\dot{b}'_{11} = d \left(\frac{r^*}{c} + \frac{2 \cdot B_2(\omega_0) \cdot c}{\pi \cdot \beta \cdot r^*} \right) \sinh Q^*$$

$$\dot{b}'_{12} = \frac{d}{\mu \cdot r^*} \left(\frac{r^*}{c} + \frac{2 \cdot B_2(\omega_0) \cdot c}{\pi \cdot \beta \cdot r^*} \right) \cosh Q^* - \frac{2 \cdot B_2(\omega_0)}{\pi \cdot \beta \cdot r^* \cdot \rho \cdot \omega} \left(2 + \frac{c^2}{\beta^2 \cdot r^{*2}} \right) \sinh Q^*$$

$$\dot{b}'_{21} = -\mu \cdot r^* \cdot d \left(\frac{r^*}{c} + \frac{2 \cdot B_2(\omega_0) \cdot c}{\pi \cdot \beta \cdot r^*} \right) \cosh Q^* - \frac{2 \cdot B_2(\omega_0) \cdot \mu \cdot \beta \cdot r^*}{\pi \cdot \omega} \left(2 + \frac{c^2}{\beta^2 \cdot r^{*2}} \right) \sinh Q^*$$

<u>third case : c=ß</u>

Here, r=Q=0. Calculations at the limit c ---> ß are required.
The layer matrix becomes:

$$b_{ij} = \begin{bmatrix} 1 & \frac{\omega \cdot d}{\mu \cdot c} \\ 0 & 1 \end{bmatrix}$$

We have:

$$\dot{b}_{11} = -\frac{\omega^2 \cdot d^2}{c^3}$$

$$\dot{b}_{12} = -\frac{\omega \cdot d}{\mu \cdot c^2} \cdot \left(1 + \frac{\omega^2 \cdot d^2}{3 \cdot c^2} \right)$$

$$\dot{b}_{21} = \frac{2 \cdot \mu \cdot \omega \cdot d}{c^2}$$

$$\dot{b}'_{11} = \frac{2 \cdot d^2 \cdot \omega \cdot B_2(\omega_0)}{\pi \cdot c}$$

$$\dot{b}'_{12} = \frac{d}{\mu} \cdot \left(\frac{1}{c} - \frac{4 \cdot B_2(\omega_0)}{\pi} \right) + \frac{2 \cdot B_2(\omega_0) \cdot \omega^2 \cdot d^3}{3 \cdot \pi \cdot \mu \cdot c^2}$$

$$\dot{b}'_{21} = -\frac{4 \cdot \mu \cdot d \cdot B_2(\omega_0)}{\pi}$$

Appendix B: Computation of the integral quantities I_1 and C_2.

The notation S-L denotes the transition from the solid to the liquid or rigid halfspace, while the classical solid halfspace will be denoted S-S. The dot symbol (·) is used here for the derivatives with respect to the time. Let us first define the integrals J^1_m, J^2_m and J^3_m.

With

$$q_m = k \cdot r_{\beta_m} \cdot (z - z_{m-1})$$

we get:

$$J^1_m = \int_{z_{m-1}}^{z_m} \cos^2 q_m \, dz$$

$$J^2_m = \int_{z_{m-1}}^{z_m} \sin^2 q_m \, dz$$

$$J^3_m = \int_{z_{m-1}}^{z_m} \sin q_m \cos q_m \, dz$$

We shall also use J^4_m, J^5_m, J^6_m and J^7_m which are defined below.
We have to distinguish three cases : $c>\beta_m$, $c<\beta_m$ and $c=\beta_m$.

For $c>\beta_m$:

$$J^1_m = \frac{d_m}{2} + \frac{c \cdot \sin(2Q_m)}{4 \cdot \omega \cdot r_{\beta_m}}$$

$$J^2_m = \frac{d_m}{2} - \frac{c \cdot \sin(2Q_m)}{4 \cdot \omega \cdot r_{\beta_m}}$$

$$J^3_m = \frac{c \cdot \sin^2 Q_m}{2 \cdot \omega \cdot r_{\beta_m}}$$

$$J^4_m = \frac{c \cdot \sin^2 Q_m}{2 \cdot \omega \cdot r^2_{\beta_m}} = \frac{J^3_m}{r_{\beta_m}}$$

$$J^5_m = r^2_{\beta_m} \cdot J^2_m \quad ; \quad J^6_m = r^2_{\beta_m} \cdot J^4_m \quad ; \quad J^7_m = \frac{J^2_m}{r^2_{\beta_m}}$$

For $c<\beta_m$:

$$J^1_m = \frac{d_m}{2} + \frac{c \cdot \sinh(2Q^*_m)}{4 \cdot \omega \cdot r^*_{\beta_m}}$$

$$J^2_m = \frac{d_m}{2} - \frac{c \cdot \sinh(2Q^*_m)}{4 \cdot \omega \cdot r^*_{\beta_m}}$$

$$J^3_m = \frac{i \cdot c \cdot \sinh^2 Q^*_m}{2 \cdot \omega \cdot r^*_{\beta_m}}$$

$$J^4_m = \frac{c \cdot \sinh^2 Q^*_m}{2 \cdot \omega \cdot r^{*2}_{\beta_m}} = \frac{J^3_m}{r^*_{\beta_m}}$$

$$J^5_m = -r^{*2}_{\beta_m} \cdot J^2_m \quad ; \quad J^6_m = -r^{*2}_{\beta_m} \cdot J^4_m \quad ; \quad J^7_m = -\frac{J^2_m}{r^{*2}_{\beta_m}}$$

For $c=\beta_m$:

$$J^1_m = d_m \quad ; \quad J^2_m = 0 \quad ; \quad J^3_m = 0$$

$$J^4_m = \frac{\omega \cdot d^2}{2c} \quad ; \quad J^5_m = 0 \quad ; \quad J^6_m = 0 \quad ; \quad J^7_m = \frac{\omega^2 \cdot d^3}{3c^2}$$

B.1. Energy Integral

The energy integral is:

$$I_1 = \int_0^\infty \rho \cdot \left(\frac{\dot{v}(z)}{\dot{v}_0} \right)^2 dz$$

For a layered medium, the energy integral can be written:

$$I_1 = \begin{cases} \left(\frac{c}{\dot{v}_0}\right)^2 \cdot \sum_{m=1}^{n} I_{(m)} & \text{for the (S - L) case} \\ \left(\frac{c}{\dot{v}_0}\right)^2 \cdot \left(\left(\sum_{m=1}^{n} I_{(m)}\right) + I_{(S-S)}\right) & \text{for the (S - S) case} \end{cases} \qquad \text{(B1)}$$

with:

$$I_{(m)} = \int_{z_{m-1}}^{z_m} \rho_m \cdot \left(\frac{\dot{v}(z)}{c}\right)^2 dz \qquad \text{(B2)}$$

$$I_{(S-S)} = \int_{z_{n-1}}^{\infty} \rho_n \cdot \left(\frac{\dot{v}(z)}{c}\right)^2 dz \qquad \text{(B3)}$$

The integrals can be written:

$$I_{(m)} = -\rho_m \cdot k^2 \cdot \left(v^2_{m-1} \cdot J^1_m + \frac{\left(y_{z_{m-1}}\right)^2 \cdot J^7_m}{k^2 \cdot \mu^2_m} + \frac{2v_{m-1} \cdot y_{z_{m-1}} \cdot J^4_m}{k \cdot \mu_m} \right)$$

$$I_{(S-S)} = \frac{\rho_n \cdot v^2_{n-1} \cdot k}{2 \cdot r^*_{\beta_n}}$$

where v_m is the displacement in the m'th layer and y_{z_m} is the stress in the m'th layer.

B.2. Phase attenuation

The coefficient C_2 is given by:

$$C_2 = \frac{\int_0^{\infty} \mu \cdot B_1 \cdot B_2 \cdot \left(\frac{y^2_z}{\mu^2 \cdot k^2} + v^2\right) dz}{c \int_0^{\infty} \mu \cdot v^2 dz}$$

C_2 can also be written:

$$C_2 = \frac{I^1 + I^2}{c \cdot I^3}$$

with:

$$I^1 = -\int_0^{\infty} \mu \cdot B_1 \cdot B_2 \cdot \left(\frac{\dot{v}}{c}\right)^2 dz = k^2 \cdot v^2_0 \cdot \int_0^{\infty} \mu \cdot B_1 \cdot B_2 \cdot \left(\frac{\dot{v}(z)}{\dot{v}_0}\right)^2 dz$$

$$I^2 = \int_0^{\infty} \mu \cdot B_1 \cdot B_2 \cdot \frac{y^2_z}{\mu^2} dz$$

$$I^3 = -\int_0^{\infty} \mu \cdot \left(\frac{\dot{v}}{c}\right)^2 dz = k^2 \cdot v^2_0 \cdot \int_0^{\infty} \mu \cdot \left(\frac{\dot{v}(z)}{\dot{v}_0}\right)^2 dz$$

To compute I^1 and I^3 we can use the same scheme as for I^2, assuming simple substitution in multiplicative coefficients:

for I^1 we shall use $(\mu_m B_{1_m} B_{2_m} k^2 v_0^2)$ instead of μ_m and
for I^3 we shall use $(\mu_m k^2 v_0^2)$ instead of μ_m.

Let us now consider I^2 for the S-L case. We obtain:

$$I^2 = k^2 \cdot \sum_{m=1}^{n} \mu_m \cdot B_{1_m} \cdot B_{2_m} L_m$$

while for the S-S case, we have:

$$I^2 = \left(k^2 \cdot \sum_{m=1}^{n-1} \mu_m \cdot B_{1_m} \cdot B_{2_m} L_m\right) - \frac{k \cdot \mu_n \cdot B_{1_n} \cdot B_{2_n} \cdot v^2_{n-1} \cdot r^*_{\beta_n}}{2}$$

The quantity L_m is given by:

$$L_m = v^2_{m-1} \cdot J^5_m + \frac{y^2_{z_{m-1}} \cdot I_{(m)}}{k^2 \cdot \mu^2_m} - \frac{2 \cdot v_{m-1} \cdot y_{z_{m-1}} \cdot J^6_m}{k \cdot \mu_m}$$

EFERENCES

1) PANZA, G. F. (1985).Synthetic seismograms: the Rayleigh waves modal ummation. J. Geophys., 58, 125-145.

2) FLORSCH, N., FAEH, D., SUHADOLC, P. and PANZA, G.F. (1989). Complete ynthetic seismograms for high-frequency multimode Love waves. ubmitted to Pure Appl. Geophys.

3) VACCARI, F., GREGERSEN, S., FURLAN, M. and PANZA, G.F. (1989). ynthetic seismograms in laterally heterogeneous, anelastic media by modal ummation of P-SV-waves. Geophys. J. Int., 99, 285-295.

4) HARKRIDER,D.G.(1964). Surface waves in multilayered elastic media. art I. Rayleigh and Love waves from buried sources in a multilayered lastic half-space. Bull. Seism. Soc. Am., 54, 627-679.

5) PANZA, G. F., SCHWAB, F. and KNOPOFF, L. (1973). Multimode surface /aves for selected focal mechanisms: I. Dip-slip on a vertical fault plane. ieophys. J. R. Astron. Soc., 34, 265-278.

6) HASKELL, N. A. (1953) The dispersion of surface waves on multilayered ıedia. Bull. Seism. Soc. Am., 43, 17-34.

7) KNOPOFF, L.(1964). A matrix method for elastic wave problems. Bull. eism. Soc. Am., 54, 431-438.

8) SCHWAB, F. and KNOPOFF, L. (1972). Fast surface wave and free mode omputations. In: Methods in computational physics. Vol 11. B.A. Bolt, ed.: p.87-180. New York, Academic Press.

9) SCHWAB, F. , NAKANISHI, K., CUSCITO, M., PANZA, G.F., LIANG, G. and REZ, J.(1984). Surface-wave computations and the synthesis of ieoretical seismograms at high frequencies. Bull. Seism. Soc. Am., 74, 1555-578.

10) SCHWAB, F. (1970) Surface-wave dispersion computations: Knopoff's ıethod. Bull. Seism. Soc. Am., 60, 1491-1520.

11) PANZA, G. F. and SUHADOLC, P. (1987). Complete strong motion ynthetics. In: Seismic strong motion synthetics. Vol 4. B.A. Bolt, ed.:pp.153-04. Orlando: Academic Press.

12) FUTTERMAN, W. (1962) Dispersive body waves. J. Geophys. Res., 67, 279-5291.

13) TAKEUCHI, H. and SAITO, M. (1972) Seismic surface wave. In: Methods ı computational physics. Vol 11. B.A. Bolt, ed.: pp.217-295. New York, .cademic Press.

14) AKI, K and RICHARDS, P. G. (1980). Quantitative seismology. Theory nd methods. Freeman and Co. San Francisco.

15) DAY, S.M., Mc LAUGHLIN, K.L., SKOLLER, B. and STEVENS, J.L. (1989) otential errors in locked modes synthetics for anelstic Earth models ieophys. Res. Let., 16, 203-206.

16) HARKRIDER, D. G. (1970). Surface waves in multilayered elastic media. art II. Higher mode spectra and spectral ratios from point sources in plane ıyered earth models. Bull. Seism. Soc. Am., 60, 1937-1987.

(17) LEVSHIN, A. L. (1985) Effects of lateral inhomogeneities on surface waves amplitude measurements, Ann. Geophys. 3, 511-518.

(18) GREGERSEN, S. and ALSOP, L. (1974). Amplitudes of horizontally refracted Love waves. Bull. Seismol. Soc. Am. 64, 535-553.

(19) HERRERA, I. (1964). A method to obtain Green's function for a multi-layered half-space. Bull. Seismol. Soc. Am. 54, 1087-1096.

(20) PANZA, G.F., SCHWAB, F. and KNOPOFF, L. (1972) Channel and Crustal Rayleigh waves. Geophys. J. R. astr. Soc., 30, 273-280.

(21) PANZA, G.F. and CALCAGNILE, G. (1974). Lg, Li and Rg from Rayleigh modes. Geophys. J.R. astr. Soc., 40, 475-487.

(22) SCHWAB, F. and KNOPOFF, L. (1973). Love waves and the torsional free modes of a multilayered anelastic sphere, Bull. Seism. Soc. Am., 63, 1107-1117.

(23) KNOPOFF, L., SCHWAB, F. and KAUSEL, E. (1973). Interpretation of Lg, Geophys. J. R. astr. Soc., 33, 389-404.

(24) KNOPOFF, L., SCHWAB, F., NAKANISHI, K. and CHANG, F.(1974). Evaluation of Lg as a discriminant among different continental crustal structures, Geophys. J. R. astr. Soc., 39, 41-70.

(25) KNOPOFF, L., AKI, K., ARCHAMBEAU, C.B., BEN-MENAHEM, A. and HUDSON, J.A. (1964). Attenuation of dispersed waves. J. Geophys. Res., 69, 1655-1657.

(26) SCHWAB, F. A. and KNOPOFF, L. (1971). Surface waves on multilayered anelastic media. Bull. Seism. Soc. Am., 61, 893-912, 1971.

(27) PATTON, H. (1980). Crust and upper mantle structure of the Eurasian continent from phase velocity and Q of surface waves, Rev. Geophys. Space Phys. 18, 605-625.

(28) ITS, E.N. and YANOVSKAYA, T.B. (1985). Propagation of surface waves in a half-space with vertical, inclined or curved interfaces, Wave Motion 7, 79-94.

(29) HEATON, T. H. and HELMBERGER, D.V. (1978).Bull. Seism. Soc. Am., 68, 31-48.

(30) SWANGER, H.J. and BOORE, D.M. (1978). Bull. Seism. Soc. Am., 68, 907-922.

(31) SUHADOLC, P., VACCARI, F. and PANZA, G.F. (1988). Strong motion modeling of the rupturing process of the November 1980 Irpinia, Italy, earthquake. In: (J. Bonnin, M. Cara, A. Cisternas and R. Fantechi, eds.) Seismic Hazard in Mediterranean regions, 105-128, Kluwer, Dordrecht.

TABLE 1. Structure FRIUL7A proposed by (11).

Thickness [km]	Density [g/cm^3]	P-wave velocity [km/s]	S-wave velocity [km/s]	Q_β
0.04	2.00	1.50	0.60	20
0.06	2.30	3.50	1.80	30
0.20	2.40	4.50	2.50	100
0.70	2.40	5.00	2.90	200
2.00	2.60	6.00	3.30	400
3.50	2.60	6.20	3.45	400
4.50	2.60	6.00	3.35	100
10.00	2.60	5.50	3.30	50
3.50	2.60	6.00	3.50	400
2.50	2.75	6.50	3.75	400
2.50	2.80	7.00	3.85	400
7.50	2.80	6.50	3.75	100
4.00	2.85	7.00	3.85	200
3.00	3.20	7.50	4.25	400
1.50	3.40	8.00	4.50	400
9.00	3.45	8.20	4.65	400

Table 2. Imperial Valley structure proposed by (29)

Layer	Thickness [km]	Density [g cm-3]	S-velocity [km s^{-1}]
1	0.95	1.80	0.88
2	1.15	2.35	1.50
3	3.80	2.60	2.40
halfspace	∞	2.80	3.70

FIGURE CAPTIONS

Figure 1. Layered model and reference system.

Figure 2. With the sign conventions defined in Figure 1, the term in Δ'_m of Equation (2) represents a plane wave whose direction of propagation makes an angle $\cot^{-1} r_{\alpha_m}$ with the +z direction when r_{α_m} is real, and a wave propagated in the +x direction with amplitude diminishing exponentially in the +z direction when r_{α_m} is imaginary. Similarly, the term in Δ''_m Equation (2) represents a plane wave making the same angle with the -z direction when r_{α_m} is real and a wave propagated in the +x direction with amplitude increasing exponentially in the +z direction when r_{α_m} is imaginary. The same applies to the terms in δ'_m and δ''_m Equation (3) with r_{β_m} substituted for r_{α_m} (see Figures 2a, 2b, 2c, 2d).

Figure 3. Source geometry and coordinate system associated with the free surface. θ is the angle between the strike of the fault and the epicenter-station direction, δ is the dip, λ is the rake and h is the source depth.

Figure 4 Geometrical scheme, in the horizontal plane, of the source-receiver system. The source, located in M, and the receiver, located in M', have the distances r and r' from the vertical boundary. The ray paths, l and l', depend on the angles of incidence ϕ and ϕ', defined through Snell's law.

Figure 5. Schematic representation of the structural model used in the computation of the synthetic seismograms in the 2-D case. Two welded layered quarterspaces, composed of n and r layers respectively, are separated by a sharp vertical discontinuity. In the model shown, H_s (s=0,1,...S) represents the depth of the s-th layer, $\alpha^{(1)}_{(z)}$, $\beta^{(1)}_{(z)}$, $\alpha^{(2)}_{(z)}$, $\beta^{(2)}_{(z)}$, $f_i(z)$ and $g_j(z)$ are respectively the P- and S-waves velocities and the eigenfunctions, stresses and displacements, for the two models.

Figure 6. Model with lined up layers. There is no difference in the elastic parameters above and below the dashed lines representing the fictitious interfaces.

Figure 7. Depth-dependence of the eigenfunctions in the proximity of the halfspace.

Figure 8. Energy exchange for both ways of propagation. The second higher mode of model C and the first higher mode of model P are considered. The two curves practically overlap. The reversibility theorem is satisfied for frequencies lower than 0.5 Hz, while the difference visible at larger frequencies, still acceptable, is due to the approximations described at the end of section 10.1.

Figure 9. Elastic and anelastic parameters of the models Continental (C) and Pamir (P).

Figure 10. Transmission of energy from model C to model P. a) Incoming fundamental mode: almost all of the energy is transmitted into the outgoing fundamental mode, while mode conversion plays just a secondary role. b) Incoming first higher mode: mode conversion becomes relevant, and to transmit all of the energy more than three outgoing modes must be taken into account. In part b) the thin solid line indicates the sum of the first three outgoing modes, while the heavy solid line is obtained by adding also the contribution of C1P3, C1P4 and C1P5.

Figure 11. Structural model FRIUL7A, after (11).

Figure 12. (a) Rayleigh-wave dispersion curves for the structural model FRIUL7A. The mode numbering is the following: 0 for the fundamental mode, 1 for the first higher mode, 2 for the second higher mode, and so on up to 154. (b) enlarged portion (modes 6-154) of part (a) showing the effect of low-velocity waveguides

Figure 13. (a) Love-wave dispersion curves for the structural model FRIUL7A. The mode numbering is the following: 0 for the fundamental mode, 1 for the first higher mode, 2 for the second higher mode, and so on up to 153.

Figure 14. Rayleigh-wave group velocities for the structure FRIUL7A. The spectrum is divided into two parts: a) Rayleigh modes 0-30, b) Rayleigh modes 31-90, c) 91-154.

Figure 15. Love-wave group velocities for the structure FRIUL7A, for themodes 0-30.

Figure 16. Rayleigh-wave energy integral I_1 for the structure FRIUL7A. The spectrum is divided into two parts: a) Rayleigh modes 0-30 b) Rayleigh modes 31-154.

Figure 17. Love-wave energy integral I_1 for the structure FRIUL7A, for the modes 0-30.

Figure 18. Ellipticity of Rayleigh modes.(0-154). The clearly visible discontinuities (e.g., at about 3 Hz) are due to the crossing of w_o through zero.

Figure 19. Rayleigh-wave quality factor Q_x for the structure FRIUL7A. The spectrum is divided into two parts: a) Rayleigh modes 0-30 b) Rayleigh modes 31-154.

Figure 20. Love-wave quality factor Q_x for the structure FRIUL7A, for the modes 0-30.

Figure 21. Coupling coefficients, for both propagation directions (CFPF and PFCF), for the fundamental mode of the continental (C) and Pamir (P) models. Heavy lines indicate the results obtained by (17), while the values obtained by (3), following two different approximations, are represented by thin lines. For each direction of propagation, the upper curve is for the approximation where reflections and transmissions are not considered at the vertical boundary, while the lower curve is computed taking reflections and transmissions into account.

Figure 22. Comparison between the observed ground displacement (top trace), the synthetic signals (middle trace) computed by (30) and synthetics computed by (2) (lowest trace) for the Brawley, 1976 earthquake as recorded at station IVC. For the synthetic signals a vertical right-lateral strike-slip point source with source duration of 1.5 s, placed on a vertical plane at 6.9 km depth, is considered. All amplitudes are normalized to a source with seismic moment of 1 dyn cm.

Figure 23. Displacement, velocity and acceleration (lower three traces), computed for a receiver placed at 30 km distance from the source. The displacement is decomposed in different sets of modes (upper three traces). It shows the contribution of the higher modes to the signal waveform. A point source with source at a depth 7 km is considered (angle strike-receiver ϕ=280°, dip δ=30° and rake λ=115°). The source rupture velocity time-function is modelled by a unit step function. All amplitudes are normalized to a source with seismic moment of 1 dyn cm. The peak displacement is in units of cm, the peak velocity in units of cm s^{-1} and the peak acceleration in cm s^{-2}.(after (3)).

Figure 24. a) Transverse component of acceleration-time series at different distances from the source (15 km, 30 km, 50 km and 100 km). A point source with source duration of 0.5 s and 7 km depth is considered (angle strike-receiver ϕ=280°, dip δ=30° and rake λ=115°). All amplitudes are normalized to a source with seismic moment of 1 dyn cm. The peak acceleration is in units of cm s^{-2} (after(3)); b) Radial component of acceleration.for an instantaneous point source (h=6 km, ϕ=68°, δ=15°, λ=75°) with seismic moment $|M_o|$=1 dyn cm as a function of the epicentral distance r; from top to bottom r=(a) 10, (b) 30, (c) 50, (d) 100 km. The maximum zero-to-peak amplitudes are normalized to one. In this and all subsequent figures, the number above each seismogram gives the peak acceleration (here in units of 10^{-22} cm/sec^2), and on the horizontal axis the time is given in seconds. The structure used is FRIUL7A.

Figure 25. Geometrical scheme of the source-receiver system used to compute the synthetic seismograms shown in fig.11. In this example, the vertical discontinuity is perpendicular to the x-z plane containing the source and the receiver (ϕ=ϕ'=0°).

Figure 26. a) Coupling coefficients used to compute the synthetic seismograms shown in fig.27a and 27b; b) Coupling coefficients used to compute the synthetic seismograms shown in Fig.27c and 27d.

Figure 27. Synthetic displacements obtained for a source-receiver distance of 100 km, according to the geometrical scheme of fig.9. Source in the C model and receiver in the P model: a) vertical component, b) radial component. Source in the P model and receiver in the C model: c) vertical component, d) radial component. The instantaneous point-source used corresponds to a

Figure 28. Synthetic displacements computed for C and P models separately, using the same source parameters of fig.27. C model: a) vertical component, b) radial component. P model: c) vertical component, d) radial component.

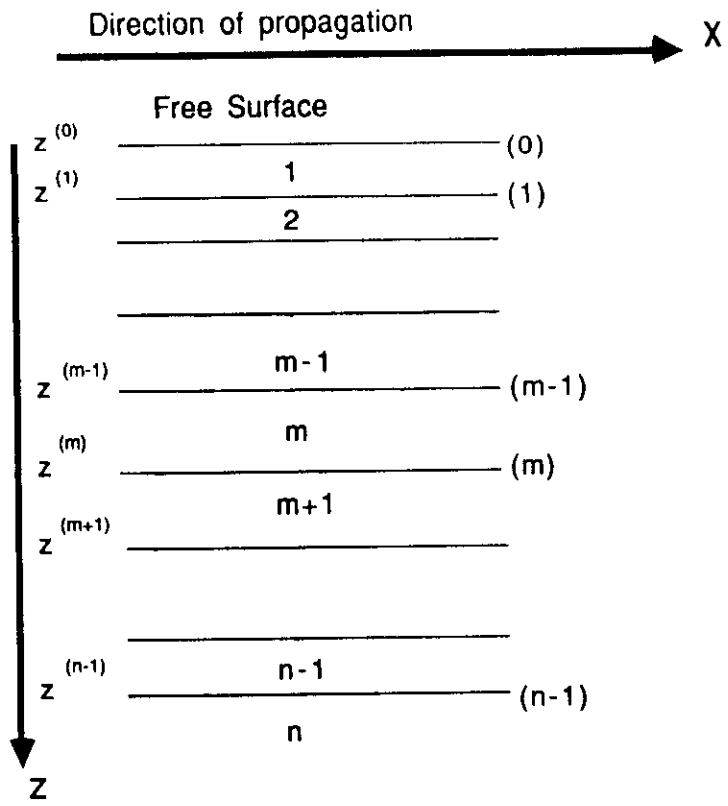

Fig. I

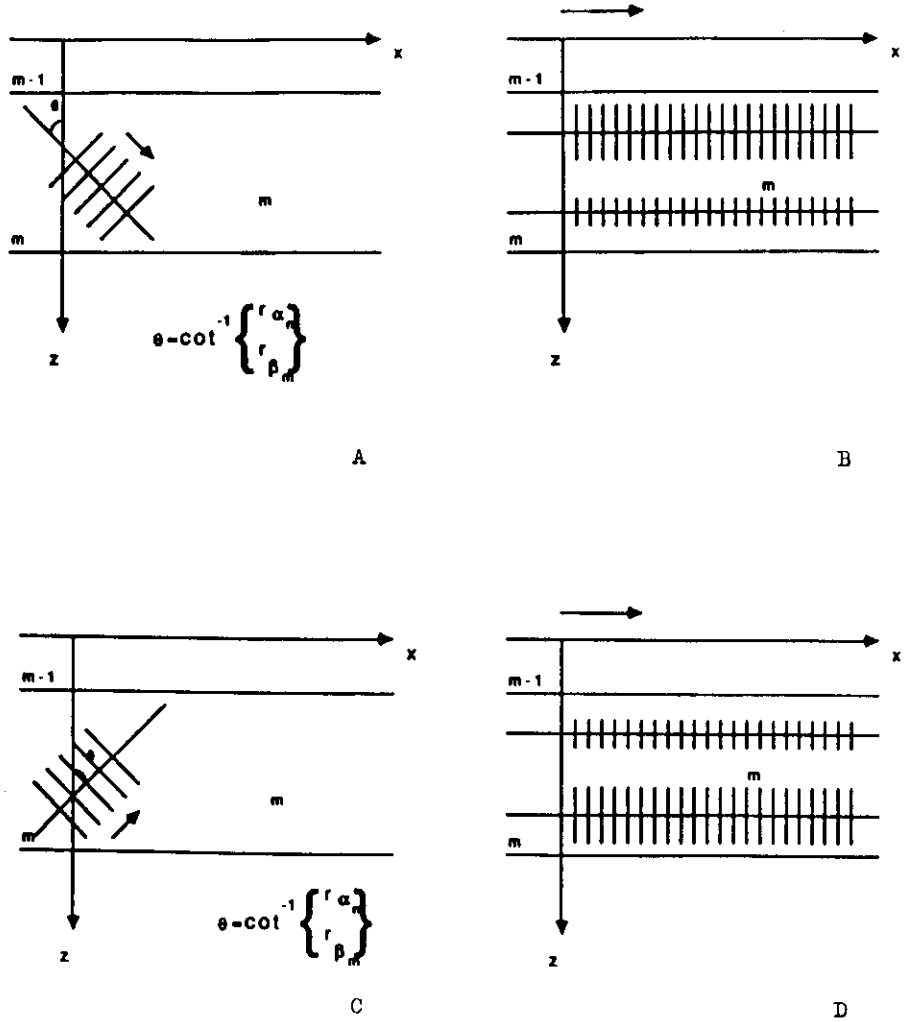
x
m-1
m
z
θ=cot⁻¹
A
B
C
D

Fig. 2

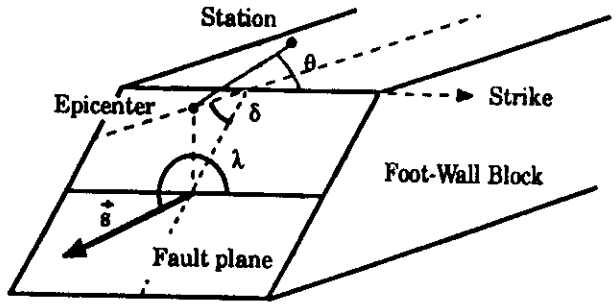
Station
θ
Epicenter
δ
Strike
λ
Foot-Wall Block
Fault plane

Fig. 3

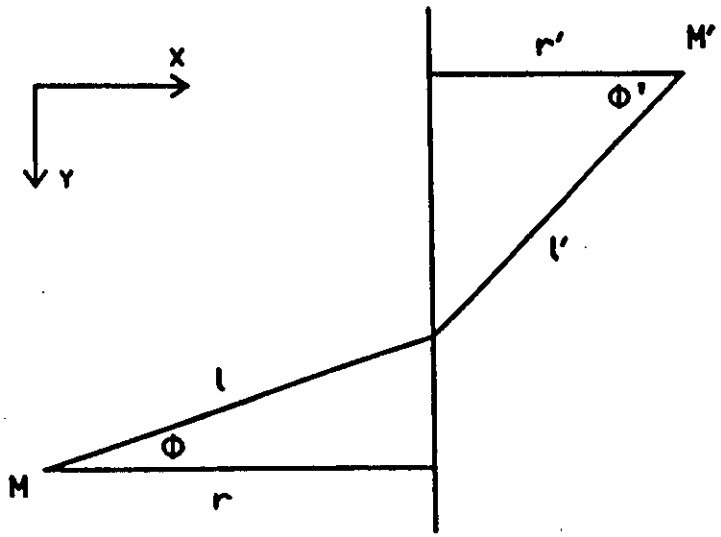

Fig. 4

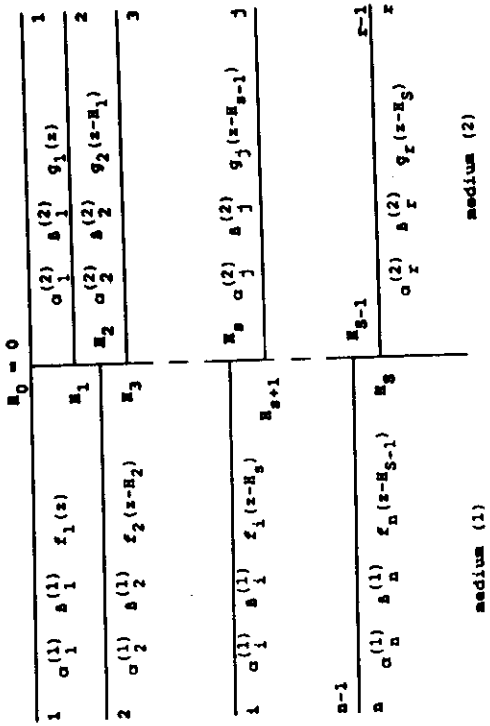

Fig. 5

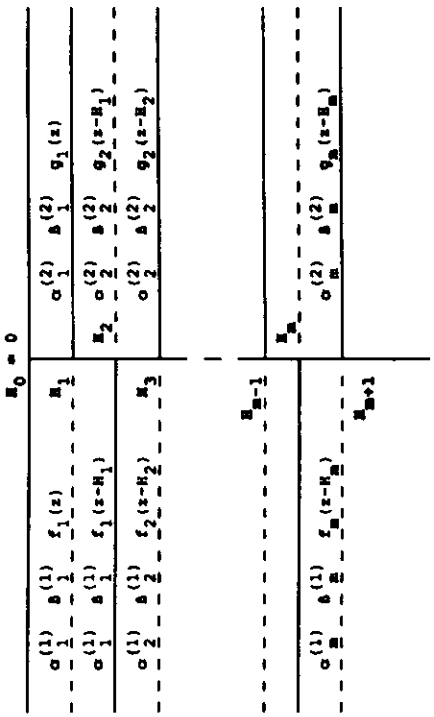
$H_0 = 0$
H_1
H_2
H_3
H_{n-1}
H_n
H_{n+1}
$\sigma_1^{(1)}$ $\beta_1^{(1)}$ $f_1(z)$
$\sigma_1^{(2)}$ $\beta_1^{(2)}$ $g_1(z)$
$\sigma_2^{(1)}$ $\beta_2^{(1)}$ $f_2(z-H_2)$
$\sigma_2^{(2)}$ $\beta_2^{(2)}$ $g_2(z-H_2)$
$\sigma_n^{(1)}$ $\beta_n^{(1)}$ $f_n(z-H_n)$
$\sigma_n^{(2)}$ $\beta_n^{(2)}$ $g_n(z-H_n)$

Fig. 6

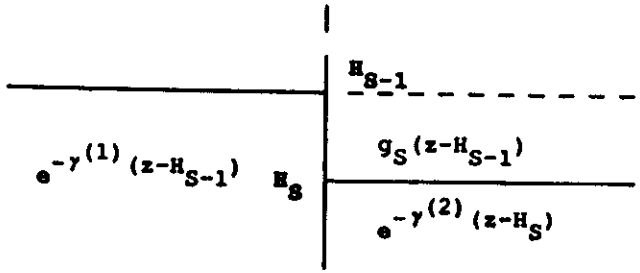
H_{S-1}
$e^{-\gamma^{(1)}(z-H_{S-1})}$
H_S
$g_S(z-H_{S-1})$
$e^{-\gamma^{(2)}(z-H_S)}$

Fig. 7

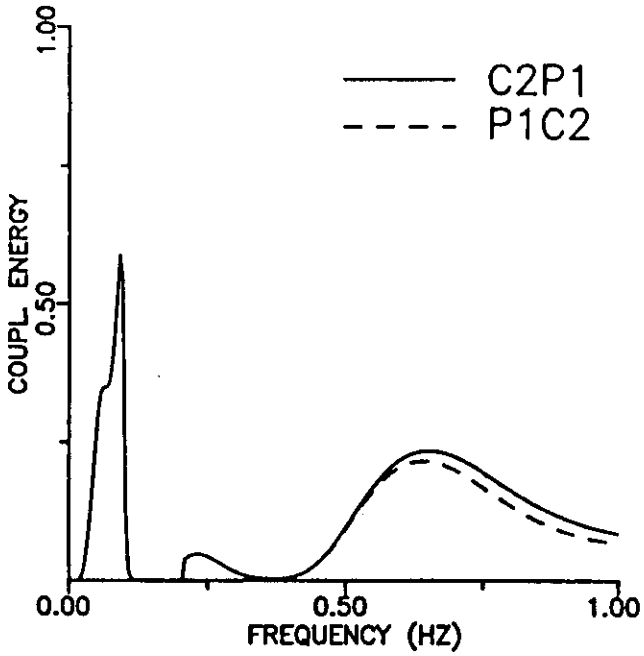
C2P1
P1C2
COUPL. ENERGY
1.00
0.50
0.00
0.50
1.00
FREQUENCY (HZ)

Fig. 8

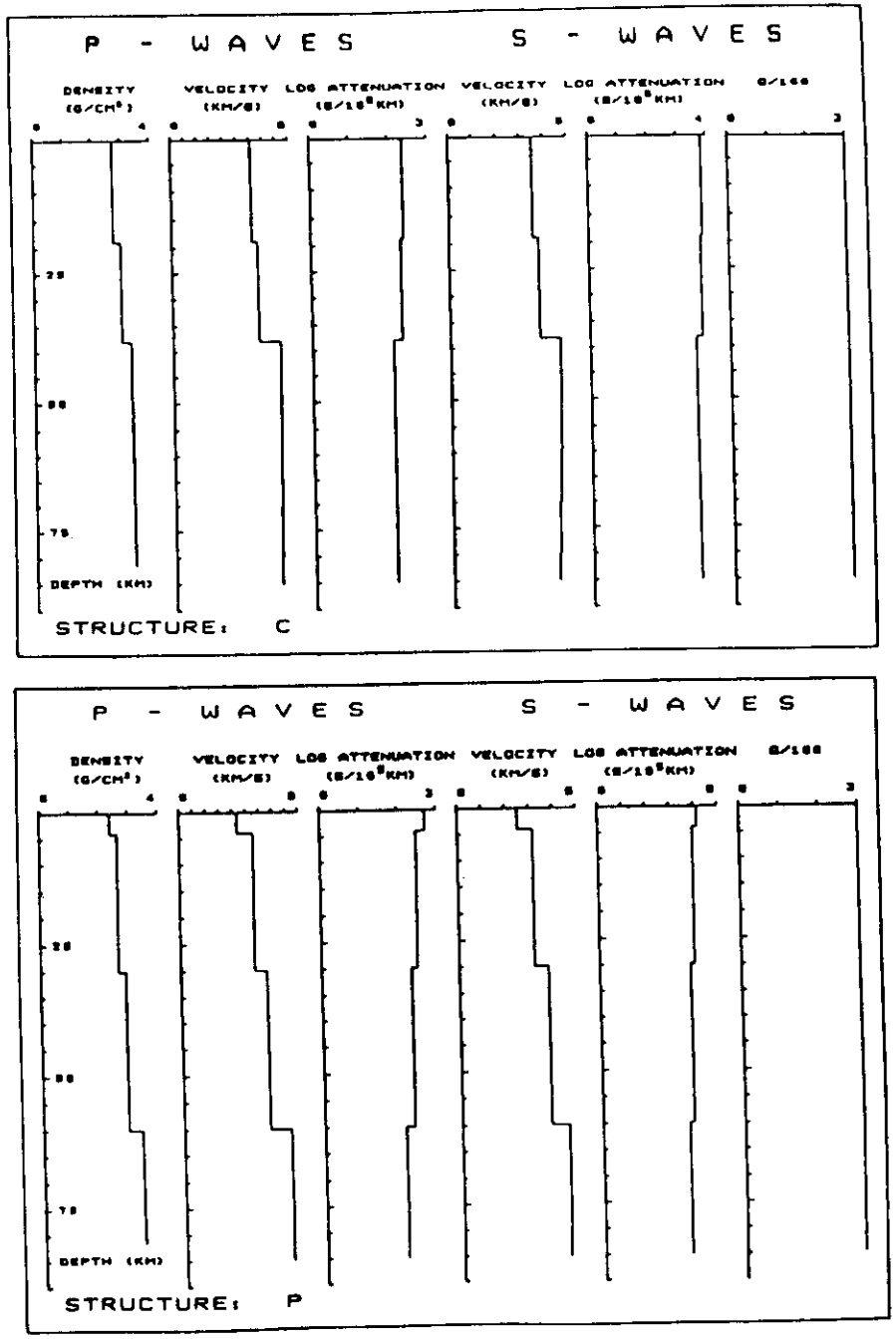
P - WAVES
S - WAVES
DENSITY (G/CM³)
VELOCITY (KM/S)
LOG ATTENUATION (S/10⁸KM)
VELOCITY (KM/S)
LOG ATTENUATION (S/10⁸KM)
G/1GS
DEPTH (KM)
STRUCTURE: C
STRUCTURE: P

Fig. 9

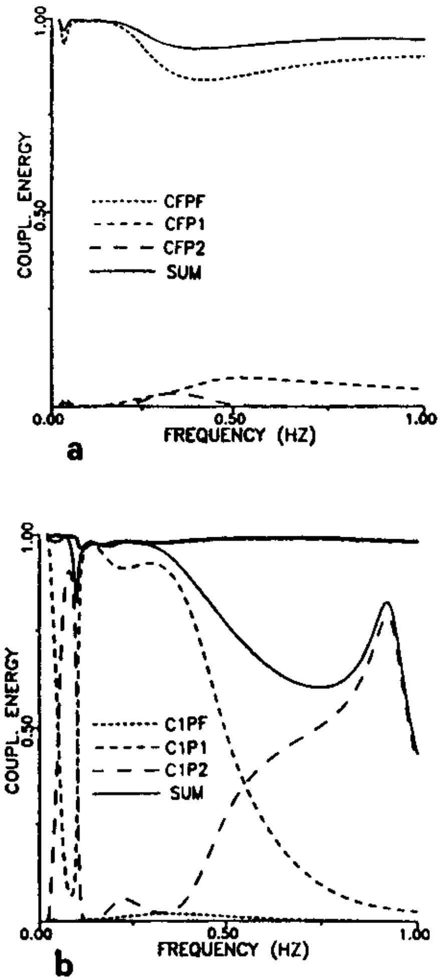

COUPL. ENERGY
FREQUENCY (HZ)
CFPF
CFP1
CFP2
SUM
a
COUPL. ENERGY
FREQUENCY (HZ)
C1PF
C1P1
C1P2
SUM
b

Fig. IO

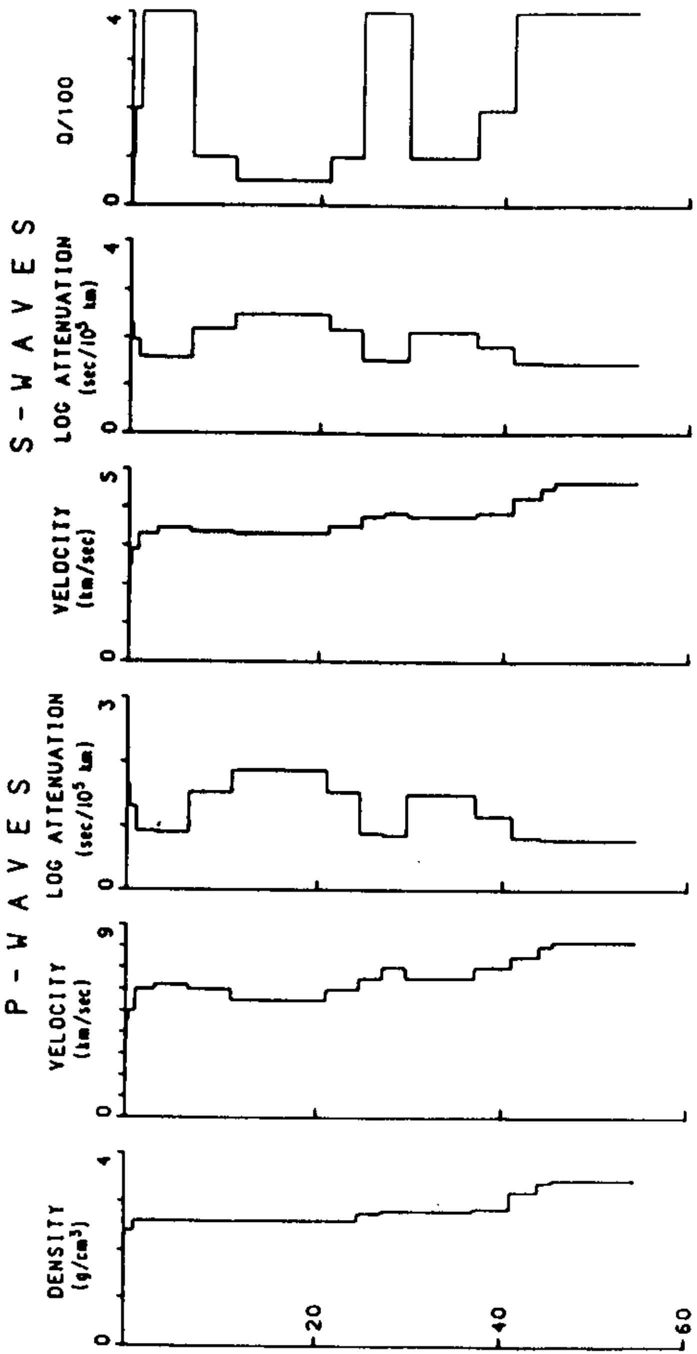

S - W A V E S
Q/100
LOG ATTENUATION
VELOCITY
P - W A V E S
LOG ATTENUATION
VELOCITY
DENSITY

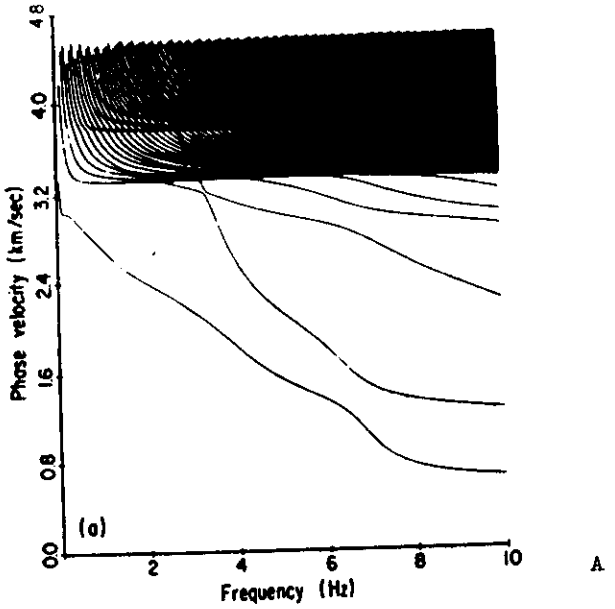

A

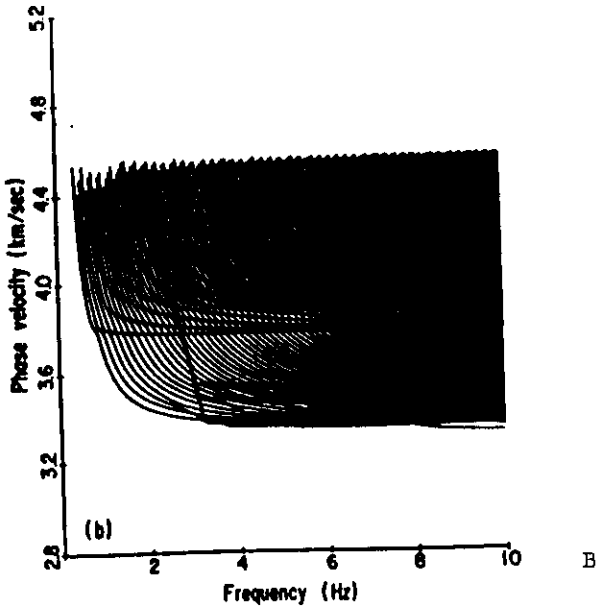

B

Fig. I2

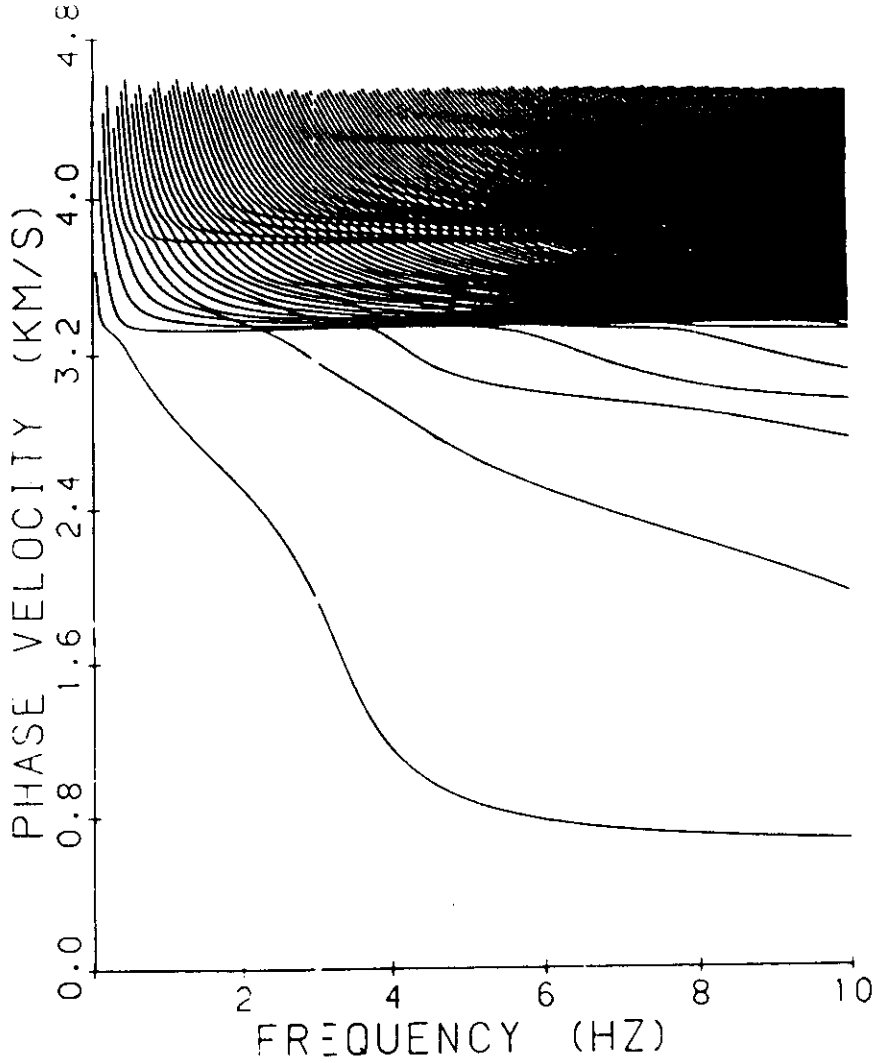

Fig. I3

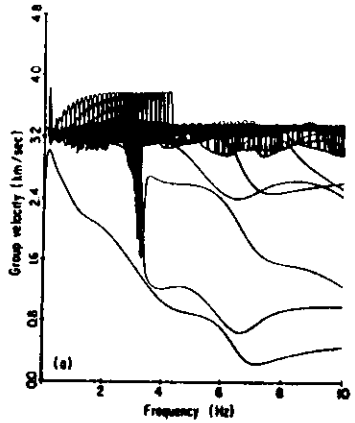

A

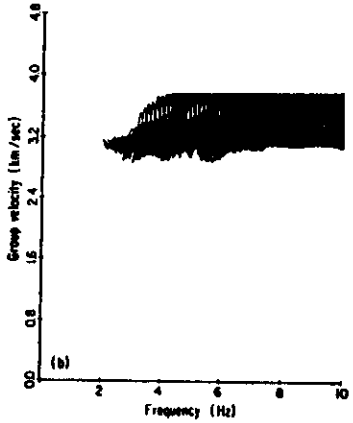

B

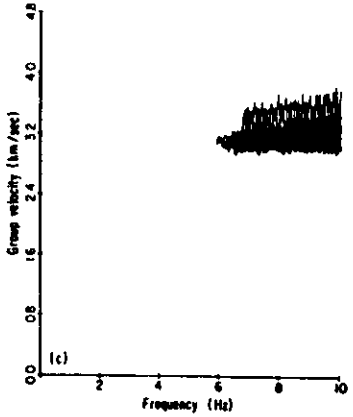

C

Fig. I4

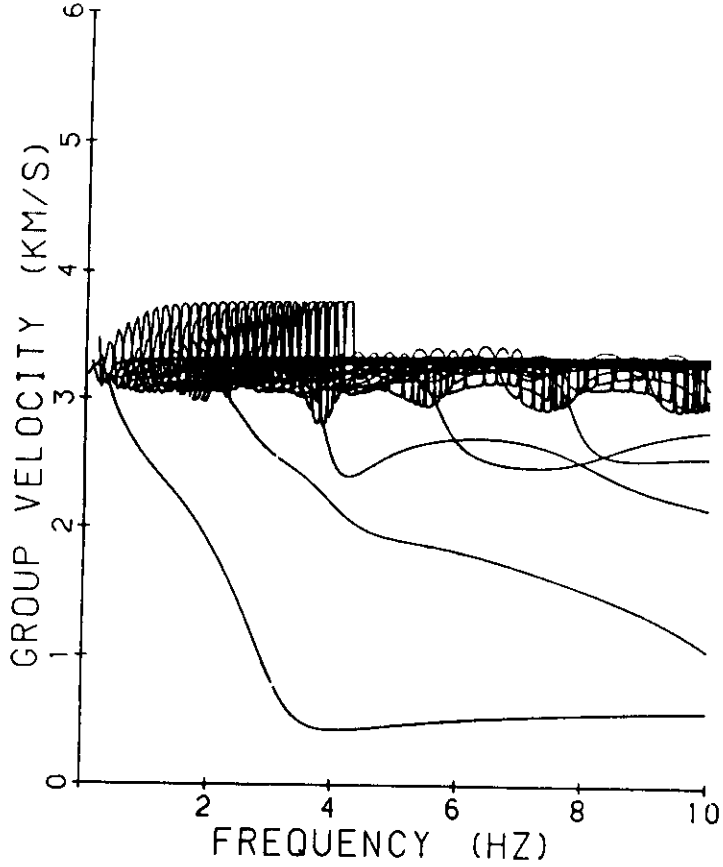

Fig. I5

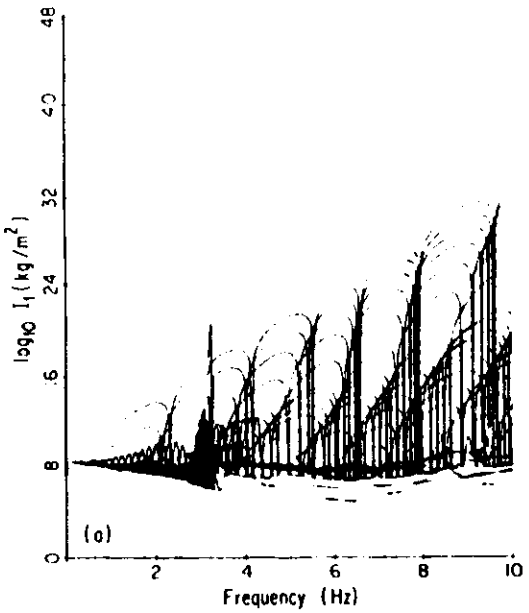

A

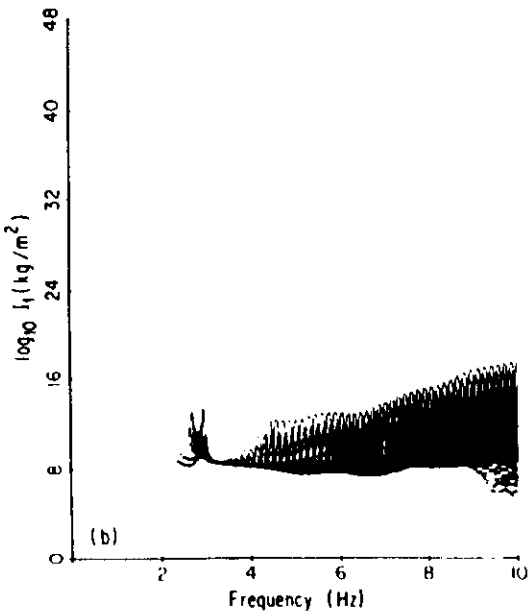

B

Fig. I6

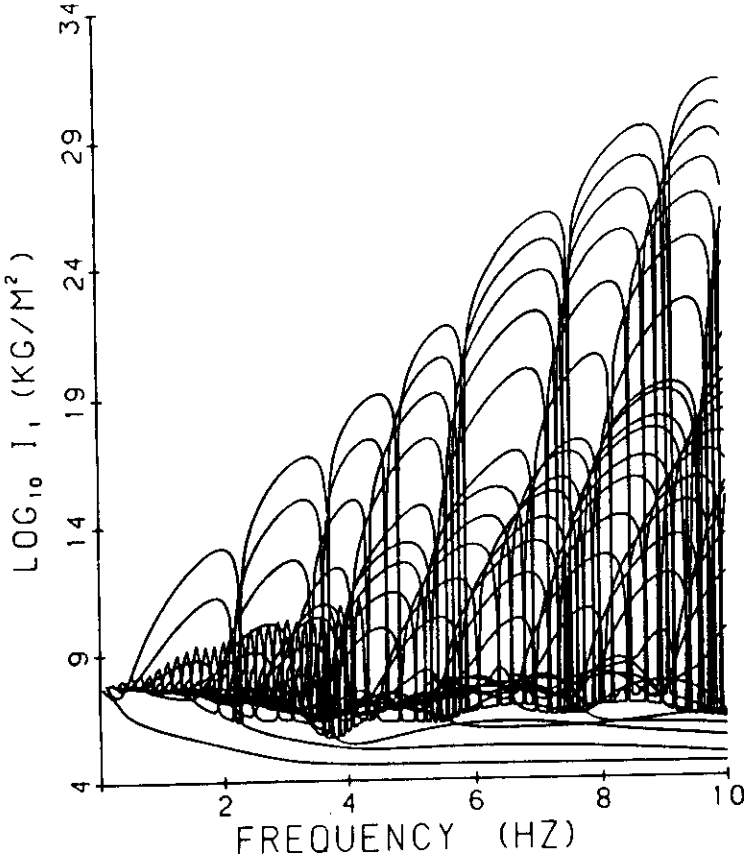

Fig. I7

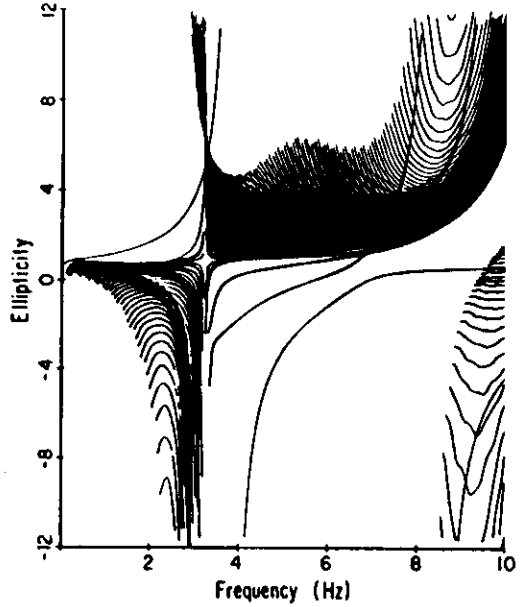

Fig. I8

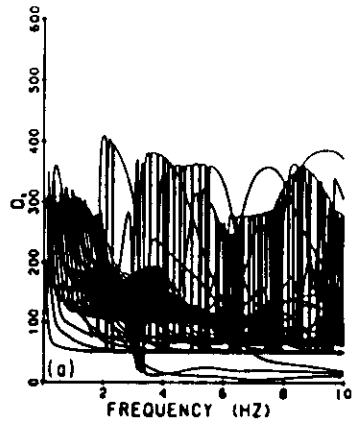

A

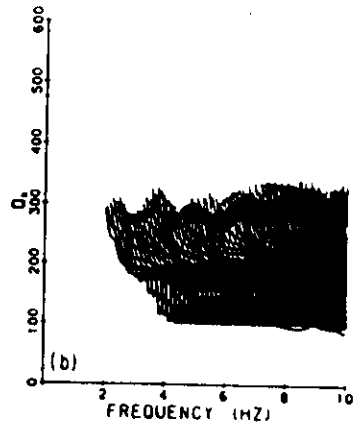

B

Fig. I9

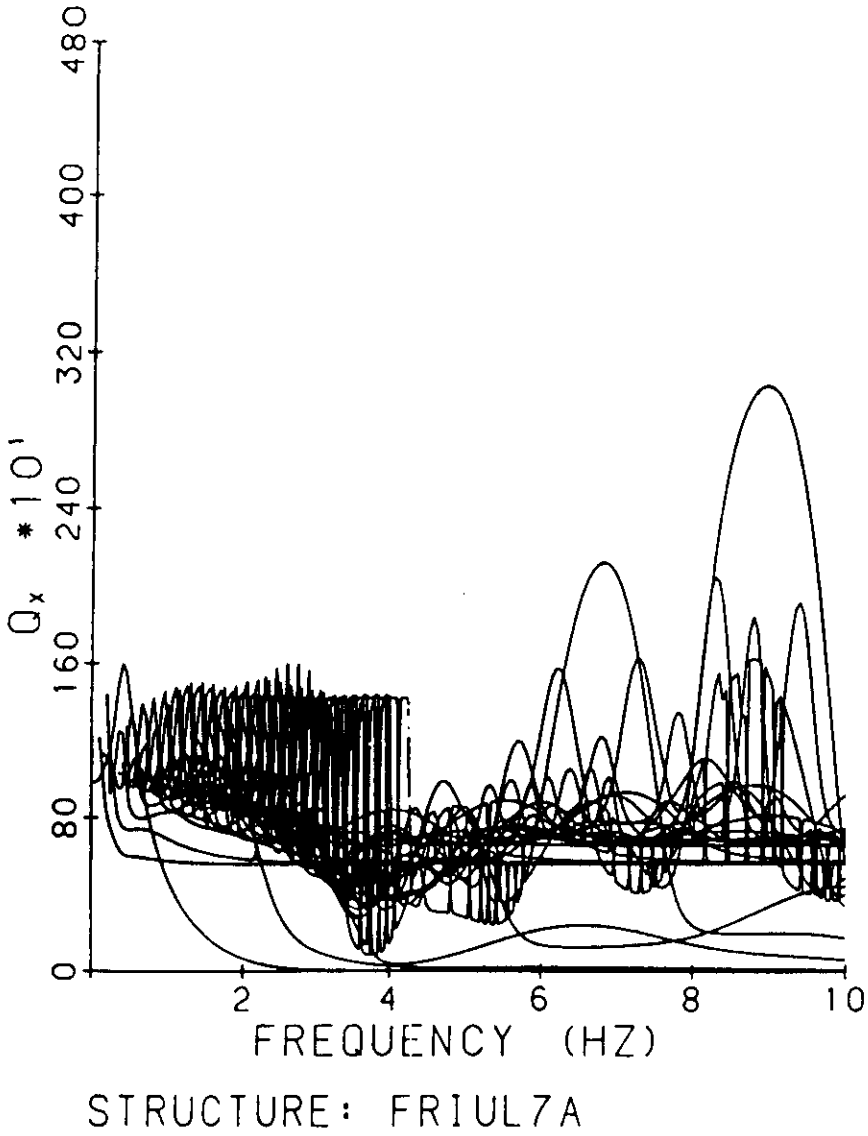
480
400
320
240
160
80
0
Q_x *10'
2
4
6
8
10
FREQUENCY (HZ)
STRUCTURE: FRIUL7A

Fig. 20

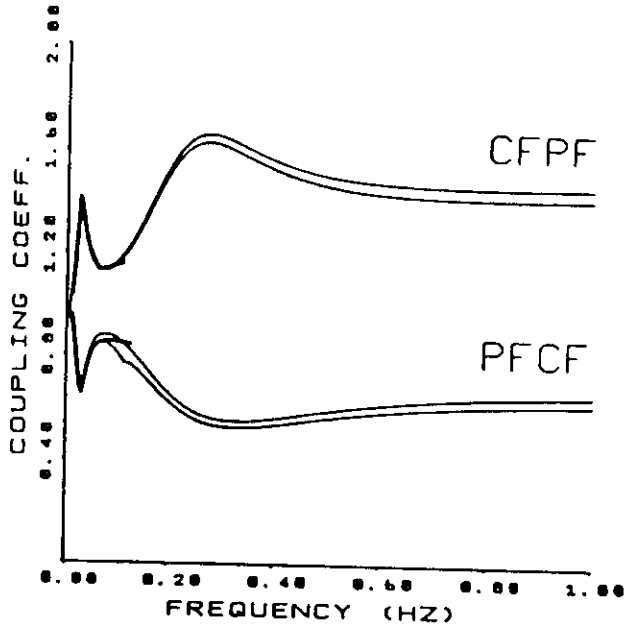
COUPLING COEFF.
CFPF
PFCF
FREQUENCY (HZ)

Fig. 2I

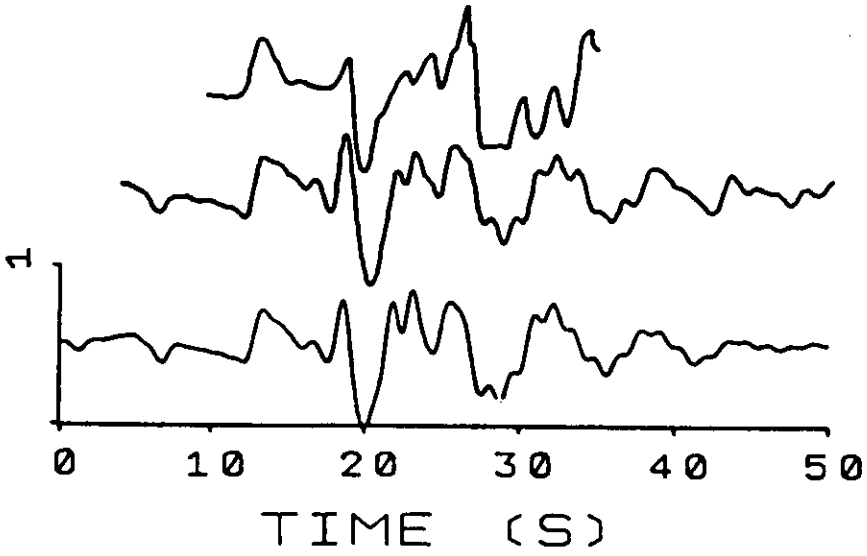
1
0
10
20
30
40
50
TIME (S)

Fig. 22

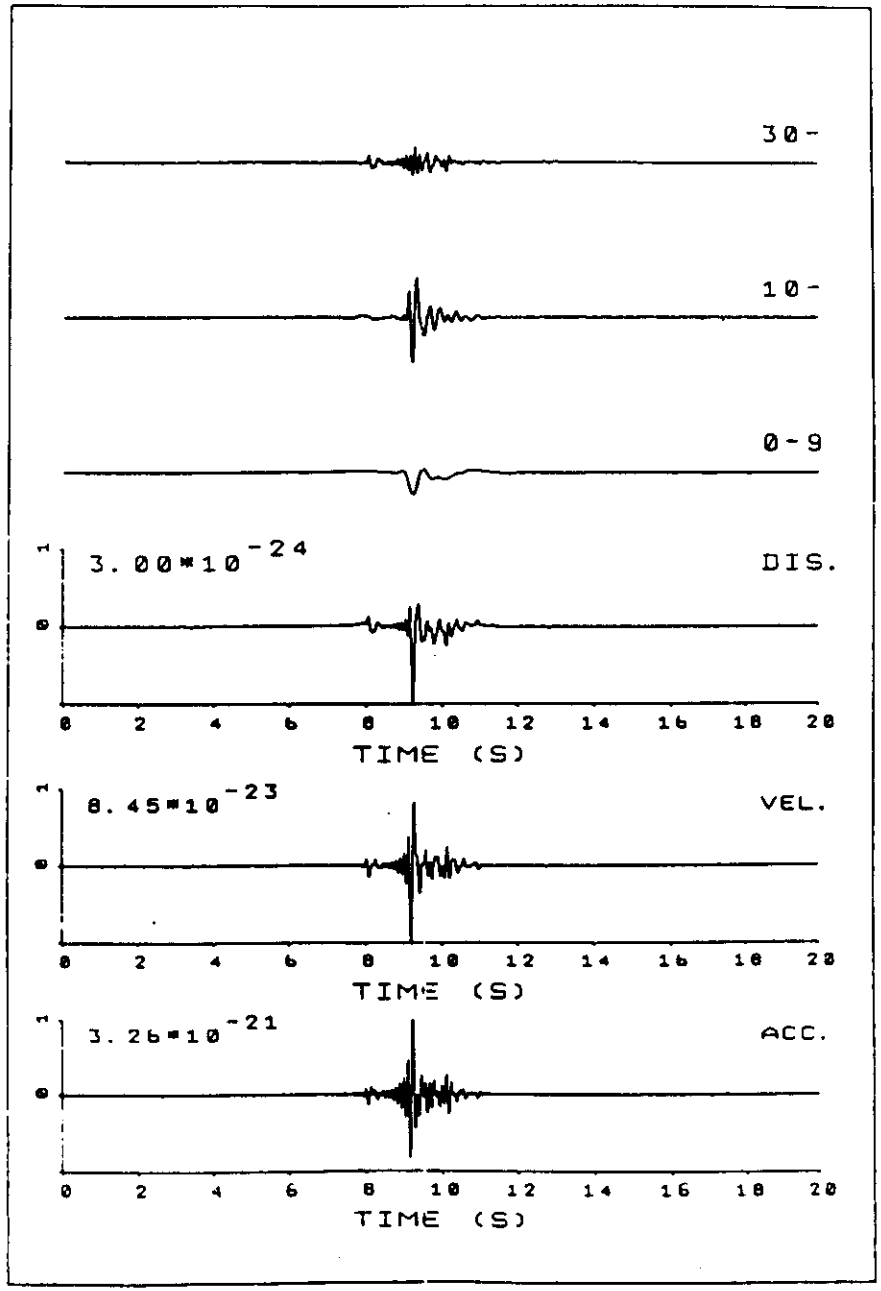
30-
10-
0-9
3.00*10^-24
DIS.
0
2
4
6
8
10
12
14
16
18
20
TIME (S)
8.45*10^-23
VEL.
TIME (S)
3.26*10^-21
ACC.
TIME (S)

Fig. 23

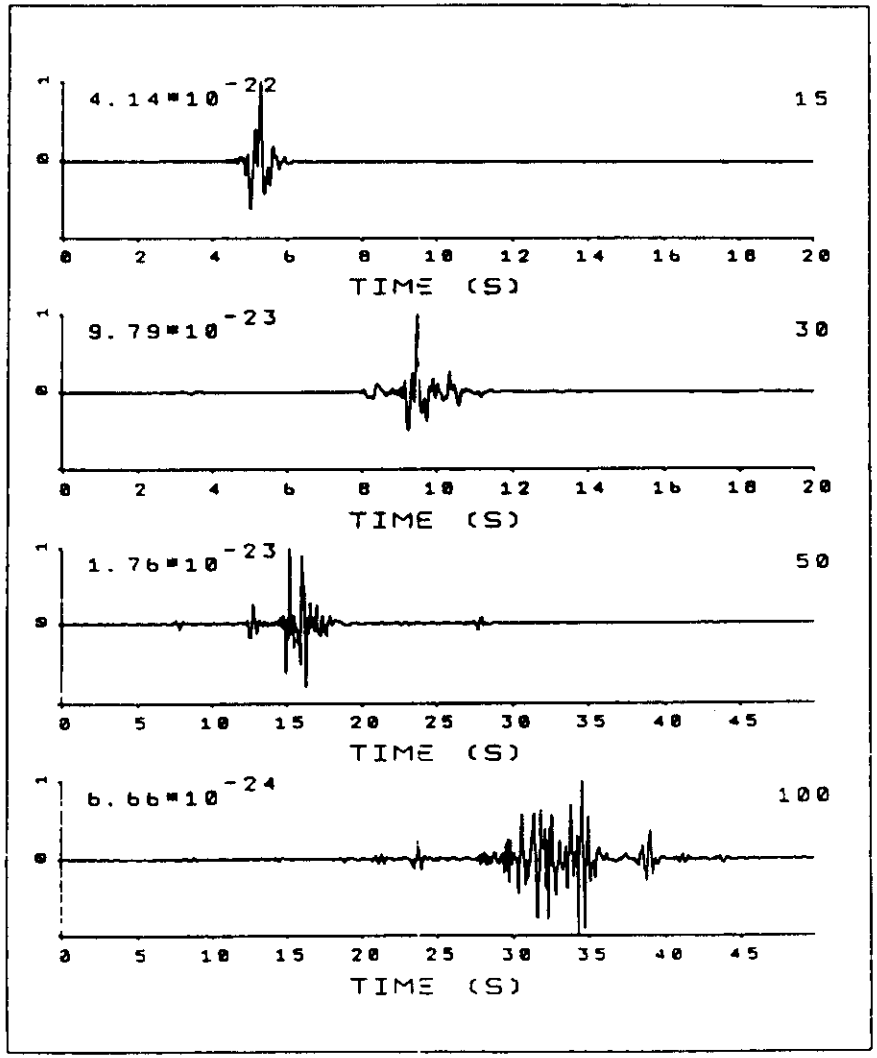

Fig. 24a

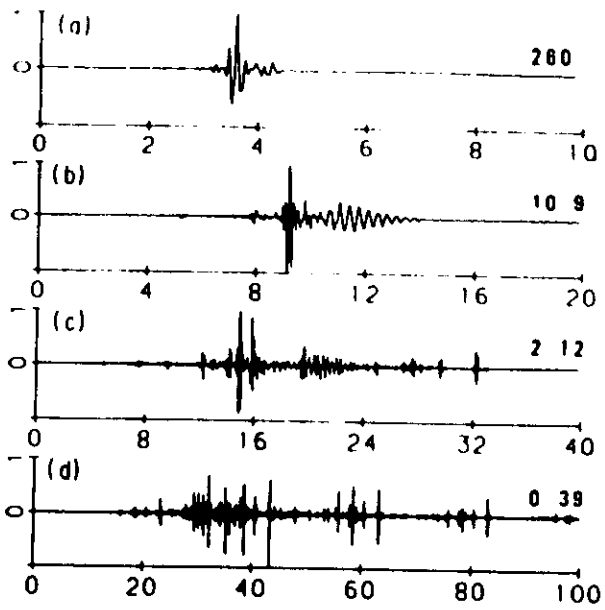

Fig. 24b

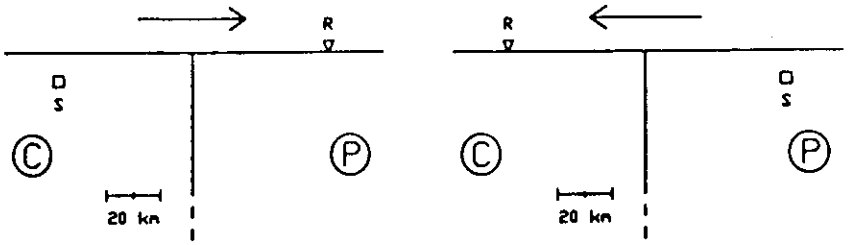
R
R
D
S
D
S
C
P
C
P
20 km
20 km

Fig. 25

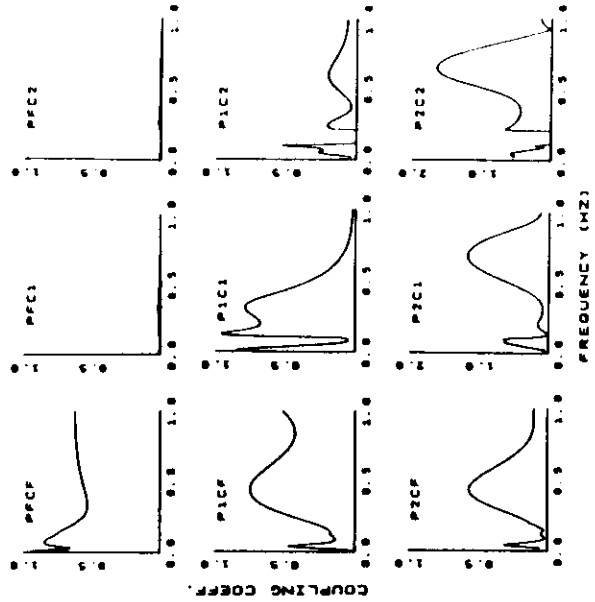
B
FREQUENCY (HZ)
COUPLING COEFF.

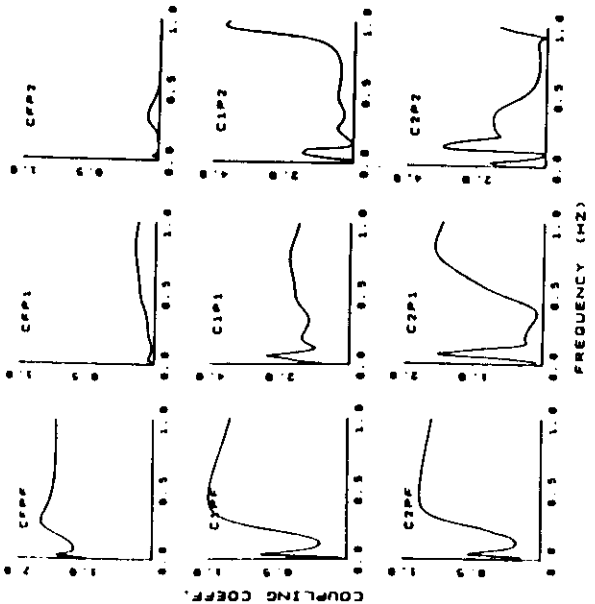
A
FREQUENCY (HZ)
COUPLING COEFF.

Fig. 26

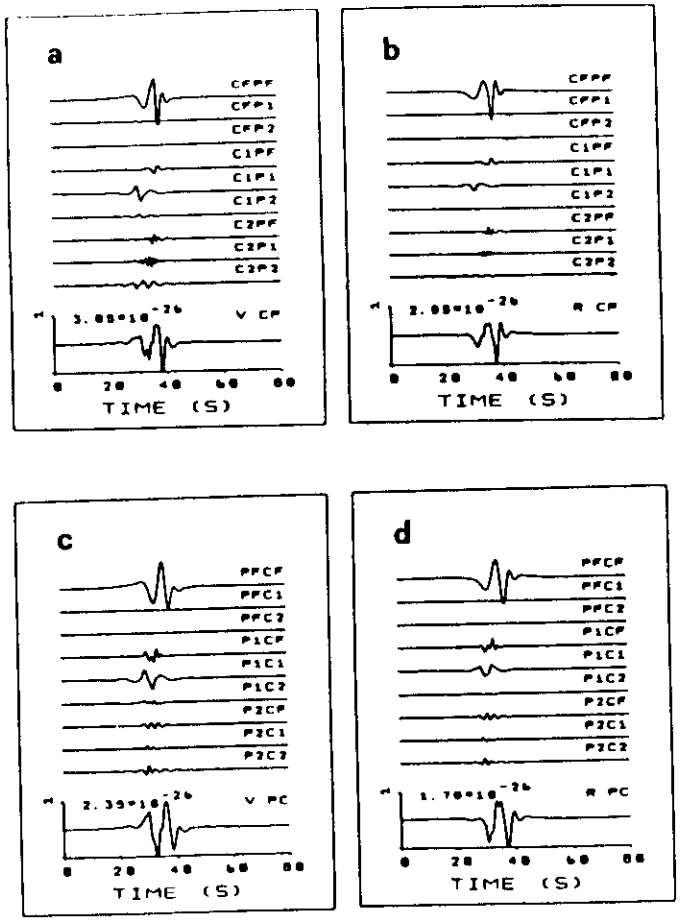

Fig. 27

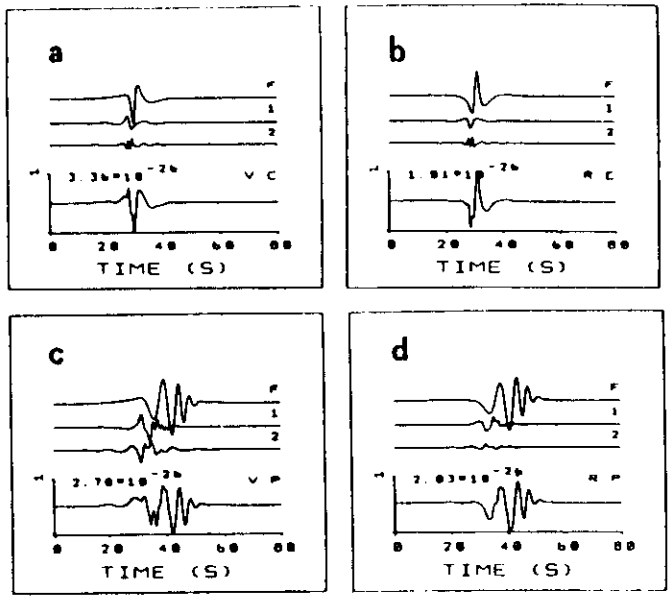

Fig. 28